Original article

Geochemical and Sr-Nd isotopic constraints on the petrogenesis and geodynamic significance of the Jebilet magmatism (Variscan Belt, Morocco)

ABDERRAHIM ESSAIFI*, SCOTT SAMSON† & KATHRYN GOODENOUGH‡

Geology Department, Cadi Ayyad University, B.P. 2390, Marrakech 40000, Morocco

†Department of Earth Sciences, Syracuse University, Syracuse, NY 13244, USA

‡British Geological Survey, Murchison House, West Mains Road, Edinburgh EH9 3LA, UK

Short title: Variscan magmatism in the Jebilet massif, Morocco

* Corresponding author, essaifi@uca.ma

Tel +212 5 24 43 46 49 (work) +212 5 24 49 05 61 (home) Fax +212 5 24 43 74 11

Abstract

In the Variscan fold belt of Morocco, the Jebilet massif is characterised by Palaeozoic metasedimentary rocks intruded by syntectonic magmatism that includes an ultramafic-to-granitoid bimodal association and peraluminous granodiorites emplaced c. 330 Ma ago, and intruded by younger leucogranites around 300 Ma. The mafic-ultramafic rocks belong to a tholeiitic series, and display chemical and isotopic signatures consistent with mixing between mantle-derived and crust-derived magmas or assimilation and fractional crystallisation. The granites within the bimodal association are mainly metaluminous to weakly peraluminous microgranites that show characteristics of A_2 type granites. The peraluminous, calc-alkaline series consists mainly of cordierite-bearing granodiorites enclosing magmatic microgranular enclaves and pelitic xenoliths. Detailed element and isotope data suggest that the alkaline and the peraluminous granitoids were formed in the shallow crust (<30 km), respectively by partial melting of tonalitic sources at high temperatures (up to 900°C), and by partial melting of metasedimentary protoliths at relatively low temperatures (~750°C). Mixing between the coeval mantle-derived and crust-derived magmas contributed to the large variation of initial εNd values and initial Sr isotopic ratios observed in the granitoids. Further contamination occurred by wall-rock assimilation during ascent of the granodioritic plutons to the upper crust. The ultramafic-to-granitoid association has been intruded by leucogranites that have high initial Sr isotopic ratios and low initial εNd values, indicating a purely crustal origin. The heating events that caused emplacement of the Jebilet magmatism are related to cessation of continental subduction and convective erosion/thinning of the lithospheric mantle during plate convergence.

Keywords: Bimodal magmatism, Peraluminous Granite, Sr-Nd isotopes, Variscan orogeny, Jebilet massif, Morocco

1. Introduction

Magmatic rocks found in orogenic belts provide a record of the thermal and chemical evolution of the deep lithospheric root of the developing orogen. During the evolution of continental collision zones, the convergence is typically first accommodated by thrusts leading to lithospheric thickening, then by crustal-scale shear zones leading to syn-convergent exhumation and lateral extrusion. Magmas of variable sources and types may be generated during the syn-convergence post-thickening period. This type of magmatism, described as post-collisional, comprises a large variety of magmatic rocks including calc-alkaline or peraluminous granitoids and alkaline type series (Lagarde *et al.*, 1992; Whalen *et al.*, 1987; 2006; Bonin, 1996), and thus is potentially informative of a range of deep crustal processes.

In the Moroccan Variscan belt, the south-western extremity of the Variscan orogen of Europe and North Africa, Variscan convergence was mainly accommodated by conjugate transcurrent shear zones that are locally associated with westward thrusting (Piqué *et al.*, 1980; Lagarde & Michard, 1986). In spite of this very limited crustal thickening numerous syntectonic calc-alkaline and peraluminous granitic plutons intruded the Cambrian to Carboniferous sedimentary formations of the Moroccan Meseta (Diot & Bouchez, 1989; Lagarde *et al.*, 1990; Gasquet *et al.*, 1996). Some of these plutons are associated with coeval mafic rocks (Fig. 1), e.g. the Tichka massif (Vogel *et al.*, 1976, Gasquet *et al.*, 1992) and Tanncherfi complex (Ajaji *et al.*, 1998) allowing evaluation of crustal- vs. mantle-derived source contributions in the genesis of the granitic magmas. The geodynamic context and the thermotectonic event that allowed crust and mantle melting in the Moroccan Meseta remain a subject of discussion. Magmatism was related to subduction and wet melting of the metasomatised mantle lithosphere of the overriding plate (Roddaz *et al.*, 2002; El Hadi *et al.*, 2006; Michard *et al.*, 2010) and /or to partial fusion of the lower crust during a postcollisional intracontinental deformation (Lagarde, 1989; Gasquet *et al.*, 1996; Hoepffner *et al.*, 2006). **In**

their general plate-tectonic evolution of the SE Variscan belt (von Raumer & Stampfli, 2008; von Raumer *et al*., 2009), the Moroccan Meseta and the Anti-Atlas represent respectively the northern and the southern margins of the Palaeotethys. This ocean was consumed during the Carboniferous by combining north-dipping subduction, dextral strike-slip and collision between Gondwana and Laurussia continents.

In the Jebilet massif, the syntectonic magmatic rocks can be divided into two main groups: a bimodal magmatic association including numerous intrusions of tholeiitic mafic-ultramafic rocks and alkaline granophyric microgranites; and calc-alkaline peraluminous granodioritic plutons cut across by leucogranitic dykes. It has been suggested that the bimodal association is mantle-derived, whereas the peraluminous granitoids largely have a source in the upper crust (Aarab & Beauchamp, 1987; Mrini *et al.*, 1992). The presence of these two magmatic groups most likely reflects a systematic interaction between the continental crust and upper mantle in this region during the Variscan orogeny.

In this paper, petrographical, geochemical and isotopic (Rb-Sr, Sm-Nd) data for the so different Carboniferous magmatic suites are integrated in order to estimate the composition of the source rocks, to constrain the petrogenesis of the varied magmatic rocks, and to evaluate tectonic models for the evolution of the Moroccan Meseta during the Late Palaeozoic time. The polymetallic (Cu, Fe, Zn, Pb) sulphide mineralisation associated with the emplacement of these magmatic suites in the Jebilet massif (Belkabir *et al.*, 2008; Essaifi & Hibti, 2008) is discussed in another paper (N'diaye *et al.*, submitted).

2. Geological setting and geology of the Jebilet magmatism

2.a. Geological setting

The Jebilet massif, located 7 km north of Marrakech, is one of the largest Palaeozoic massifs of the Variscan fold belt of Morocco. Together with the Rehamna and the central Palaeozoic massifs northward, and the high Atlas Palaeozoic block southward, it constitutes the western Meseta, which is separated from the eastern Meseta by the folded Mesozoic-Cenozoic cover of the middle Atlas (Fig. 1a). The Mesetas display a nearly complete Palaeozoic sedimentary sequence, folded and metamorphosed at greenschist to amphibolite facies, and intruded by widespread syn- to late- orogenic Carboniferous granitoids. The granitoids of the Mesetas can be grouped into three main groups (Vogel *et al.*, 1976, Gasquet *et al.*, 1996; El Hadi *et al.*, 2006) (1) calc-alkaline biotite +/- cordierite granodiorites, locally with associated mafic magmas (2) two-mica leucogranites, and (3) **subalkaline to** alkaline granites. The calc-alkaline granodioritic plutons are dominant (e.g. Jebilet, Aouli BouMia, Tanncherfi; Fig. 1a). They display I-type or mixed S- and I-type characteristics **($0.703 < Sri < 0.711$; $-6.7 < \varepsilon Nd < +7.4$)** and they are locally associated with mantle-derived basic magmas (e.g. Tichka pluton, Fig. 1a). **Among these calc-alkaline granitoids, subduction-related plutonic rocks have been recognised in the Tanncherfi plutonic complex where coeval potassic (shoshonitic) and sodic (granodioritic) calc-alkaline series, with LILE and LREE enrichment and Nb, Ta, Ti depletion, were emplaced (Ajaji *et al.*, 1998).** The leucogranites are typical S-type granites **($0.707 < Sr_i < 0.718$; $-10.7 < \varepsilon Nd < -1.5$)** derived from metasedimentary source rocks (Mahmood & Bennani, 1984; Mrini *et al.*, 1992). They are intrusive into the granodiorites (e.g. Zaer pluton, Fig. 1a) or into Lower Palaeozoic metasediments (e.g., Oulmes pluton, Fig. 1a). **The subalkaline to alkaline granites ($0.704 < Sri < 0.707$; $-4.9 < \varepsilon Nd < 0.6$) result from mixing between crust- and mantle-derived magmas (Gasquet *et al.*, 1996). They are associated with mafic rocks and coeval with the calc-alkaline granites (e.g., Tichka massif) or intrusive into Lower Palaeozoic metasediments (e.g. Rehamna, Fig. 1a)**.

In the Jebilet massif, Carboniferous magmatism includes, in addition to two cordierite-bearing granodioritic plutons intruded by leucogranites, a compositionally bimodal association of alkaline microgranites and mafic-ultramafic intrusions (Bordonaro *et al.*, 1979; Gasquet *et al.*, 1996). The spatial distribution is limited to the west by a NNE–SSW dextral thrust-wrench shear zone (Le Corre & Bouloton, 1987; Mayol & Muller, 1985) separating the central Jebilet unit, a schistose and metamorphosed block of marine Visean shales (Sarhlef schists), from the western Jebilet, a weakly deformed to undeformed block of Cambro-Ordovician limestones, shales and sandstones (Fig. 1b) (Huvelin, 1977). To the east, the granodioritic plutons are spatially associated with a NNW-SSE sinistral wrench shear zone (the Marrakech Shear Zone, Lagarde & Choukroune, 1982; Essaifi *et al.*, 2001) corresponding to the boundary with the eastern Jebilet, a weakly metamorphosed to unmetamorphosed block of Upper Visean syntectonic "flysch" with olistostromes and inliers of Ordovician-Devonian sedimentary rocks (Huvelin, 1977; Beauchamp *et al.*, 1991). These two shear zones are located in the southern prolongation of the western Meseta shear zone (WMSZ, Fig. 1a), which is the western boundary of the Carboniferous basins of the Moroccan Meseta (Piqué *et al.*, 1980). Westphalian-Permian continental conglomerates (Huvelin, 1977) rest unconformably upon the Hercynian folded sequence.

Both the cordierite-bearing granodioritic plutons and the bimodal plutonic suite intrude weakly metamorphosed (lower greenschist facies) marine metapelites dated to Upper-Middle Visean (Huvelin, 1977; Playford *et al.*, 2008). Structural studies of the Jebilet plutons and the surrounding rocks have provided evidence of syntectonic emplacement at high crustal levels for both the bimodal association and the granodioritic plutons (Le Corre & Saquaque, 1987; Lagarde *et al.*, 1990; Essaifi *et al.*, 2001). Regional metamorphism was contemporaneous with ductile deformation developed during Late Carboniferous crustal shortening, associated with the main Variscan tectonic event in Morocco (Hoepffner *et al.*, 2006; Michard *et al.*, 2010). The bimodal intrusions and the granodioritic plutons have induced in the surrounding metapelites a low-pressure contact metamorphism that reaches the hornblende- and the pyroxene-hornfels facies, respectively (Figs. 2a, b). Near the boundaries with the host rocks, numerous cm- to km-scale enclaves of the contact hornfels exist in the eastern Jebilet granodioritic pluton. The contact metamorphism paragenesis suggests that the plutons were emplaced at less than 2.2 kb corresponding to a maximum depth of 8 km (Bouloton, 1992). Leucogranitic dykes and stocks cut across the granodioritic plutons and their host rocks. Triassic microdioritic dykes post-date the Variscan deformation and cut both the bimodal association and the granodioritic plutons. They contain numerous types of enclaves, particularly of the Proterozoic rocks (Huvelin, 1977; Bouloton & Gasquet, 1995; Dostal *et al.*, 2005) that constitute the basement of the Variscan fold belt of Morocco (Michard, 1976; Piqué *et al.*, 1993).

2.b. Geology of the Jebilet Carboniferous magmatism

At the present level of exposure, the bimodal association in the Jebilet massif comprises mafic to ultramafic plutons (peridotites and gabbros) with alkaline microgranitic stocks and dykes, and volumetrically insignificant intermediate rock types (quartz diorites) that are found at gabbro/granitoid contacts, and may represent zones of magma mixing. Thin aplitic to perlitic rhyolites and rhyodacitic volcaniclastic rocks are also found in the Sarhlef schists (Bordonaro *et al.*, 1979; Aarab & Beauchamp, 1987). The calc-alkaline granodiorite plutons form two larger plutons.

2.b.1. Bimodal association

The bimodal plutonism (> 65% mafic-ultramafic, the remainder is felsic) occurs as numerous felsic and mafic intrusions of some hundreds of metres in thickness and a few kilometres in length (Fig. 1b). They are arranged into three N-S to NE-SW lineaments that are broadly parallel to local shear zones.

The mafic-ultramafic rocks include mafic to ultramafic cumulates (gabbros, peridotites) forming stock or sill-like layered intrusions showing cm-scale banding, and dolerite dykes which cut across both the intrusions and the country rocks (Fig. 3a-c). Deformation within these intrusions is very heterogeneous, and subvertical cm- to m-scale shear zones with strong planar fabrics enclose lenticular domains of sub-isotropic gabbros. The Kettara intrusion is a stratified sill composed of a lower banded series of ultramafic cumulates cut by an upper series of mafic cumulates (massive and layered leucogabbros) (Fig. 3a). In the undeformed rocks, magmatic textures are preserved in spite of an incipient to moderate recrystallisation. The magmatic minerals include olivine, clinopyroxene, plagioclase, spinel, ilmenite, apatite and quartz, while minerals related to later alteration include amphibole, chlorite, muscovite, serpentine, epidote, prehnite, anatase and calcite. The cumulate rocks are medium- to coarse-grained with ortho- to mesocumulate textures. The ultramafic cumulates are peridotites with olivine and chromian spinel as the cumulus phases, and plagioclase, clinopyroxene and ilmenite as the intercumulus phases. The mafic cumulates are leucogabbros with olivine and plagioclase as the cumulus phases while clinopyroxene and ilmenite form the intercumulus phases. Minimum crystallisation temperatures for the mafic-ultramafic cumulates were estimated from the clinopyroxene geothermometer (Lindsley & Anderson, 1983) at 1000-1100 °C (Essaifi, 1995). The non-cumulate mafic rocks form gabbros and dolerites with ophitic and subophitic textures, respectively. The gabbros vary from olivine gabbros and ilmenite-rich gabbros to quartz gabbros, while the dolerites range from olivine-bearing to quartz-bearing dolerites (Aarab & Beauchamp, 1987). Mafic-ultramafic cumulates are also present in the majority of the other intrusions of the bimodal association. In the El Mna composite intrusion (Fig. 1b), mafic-ultramafic rocks crop out in the western part of the intrusion while intermediate-felsic rocks form the eastern part.

The felsic rocks of the bimodal association crop out as metre-wide dykes enclosing mafic enclaves within the mafic-ultramafic intrusions (Fig. 3d-e) or as stocks within composite mafic-felsic intrusions (e.g. Oled Har, El Mna). They also form elongated and stretched intrusions of more than 10 km in length and less than 700m wide in a western lineament composed of the Koudiat Bouzlaf, Hamra and Diab intrusions (the "BHD" intrusions, Fig. 2a). They consist of microgranitic rocks that contain crosscutting mafic dykes (synplutonic dolerites; Fig. 3g) and leucocratic microgranular enclaves. These granitoids are locally highly deformed and have been metasomatically altered to gneissic trondhjemites and tonalites (Essaifi *et al.*, 2004a). The less deformed granitoids are observed near the boundaries with country rocks where deformation is heterogeneous. They are monzonitic microgranites that have millimetre-scale phenocrysts in a micrographic to granophyric groundmass showing a weak planar fabric. The primary minerals include quartz, plagioclase, microcline, biotite, and amphibole as essential minerals, and fluorite, apatite, zircon, ilmenite and allanite as accessory minerals. The phenocrysts are quartz, euhedral plagioclase and aggregates of Cl- and Fe-rich biotite (annite) and blue-green amphibole (hastingsite-ferropargasite). The groundmass is composed of quartz aggregates, plagioclase and microcline showing micrographic and granophyric (spherolitic) associations. Plagioclase phenocrysts in these weakly altered microgranites are sericitised (phengitic muscovite), while biotite is partially replaced by chamosite or by pumpellyite and ilmenite is altered to leucoxene.

Intermediate rocks (quartz-diorites) are present in some composite intrusions where they are localised at the contact between the felsic and the mafic-ultramafic rocks. In these intrusions field evidence, including cross-cutting relationships between intrusions of differing compositions, net veining structures and magma mixing/mingling features, indicates contemporaneous emplacement of the felsic and mafic magmas (Fig. 3f). In the El Mna intrusion (Fig. 1b), the quartz-diorite exhibits a coarse (up to 5 cm) pegmatitic texture and contains plagioclase, amphibole, biotite, K-feldspar, quartz, calcite, chlorite, ilmenite, leucoxene, apatite and zircon. The rock is characterised by abundant (30-40 vol%) cm-scale acicular amphibole (ferro-hornblende) which is partially or completely replaced by biotite and chlorite, and contains inclusion trails of ilmenite. Plagioclase is present as subhedral crystals altered into calcite and sericite. Biotite can reach 25% of the total rock volume, and some biotite crystals have inclusions of zircon. The groundmass contains quartz that invades K-feldspar (microcline) leading to formation of secondary granophyric associations. Apatite occurs as inclusions in the other phases.

A $330.5^{+0.68}_{-0.83}$ Ma age was obtained for a microgranitic sample of the BHD intrusions by U-Pb dating of zircon using the ID-TIMS technique (Essaifi *et al.*, 2003).The gabbroic rocks have not been dated, but, as mentioned above, field evidence demonstrates contemporaneous emplacement of felsic and mafic magmas.

2.b.2. Granodioritic plutons

There are two main cordierite-bearing granodioritic plutons in the area, the eastern and central Jebilet plutons. Within the country rocks, tightening of folds in the metamorphic aureole indicates an increase of strain intensity towards the pluton boundaries (Le Corre & Saquaque, 1987; Lagarde *et al.*, 1990). In the northern contact aureole of the Eastern Jebilet Pluton, injection of granitic magma occurs either perpendicular to, or along the stratification plane. Within the plutons strain is generally low, and the pre-full-crystallisation planar fabric is weak or absent (Boummane & Olivier, 2007), but strain intensity increases towards the pluton margins where a well-defined planar fabric is present and S/C structures are frequent. Ultramylonites are developed in km- to m-scale shear zones within the plutons. The two plutons are essentially composed of porphyritic biotite +/- cordierite-bearing granodiorite, but modal compositions range from monzogranites to tonalites (A. Chemesseddoha, unpub. Ph.D. thesis, Univ. Rennes I, Rennes, 1986; M. K. Ben Salah, unpub. Ph.D. thesis, Univ. Cadi Ayyad, Marrakesh, 1989; El Amrani El Hassani, 1996). The granodiorite is composed of K-feldspar megacrysts (2-3 cm) enclosed in a mesostasis (3-7mm) of biotite, plagioclase, K-feldspar, cordierite and quartz. Biotite and muscovite +/- tourmaline-bearing leucogranites are also present at the boundaries between the plutons and the country rock, or as dykes and stocks that cut across the granodiorite. The leucogranites are affected by cm-scale shear zones with a mylonitic fabric.

Two types of enclaves are found in the plutons (i) homogeneously distributed mafic microgranular enclaves with a tonalitic to dioritic composition (Fig. 3h), interpreted as resulting from mingling between a mafic, mantle-derived magma and the granodioritic magma (El Amrani El Hassani, 1996), and (ii) aluminous and ferromagnesian xenoliths (made up of aluminosilicates, cordierite, garnet, spinel, biotite, and feldspars) present mainly in the Eastern Jebilet Pluton (Fig. 3i). Hydrothermal alteration is marked in the granodioritic plutons by transformation of biotite into chlorite, K feldspar into muscovite and plagioclase into sericite, while cordierite is altered into pyrophyllite, pinnite and chlorite. The leucogranites are locally affected by extensive alteration leading to total disappearance of feldspar and development of greisens composed of quartz, muscovite and tourmaline.

In the granodioritic plutons, Mrini *et al.* (1992) obtained an isochron at 327+/-4 Ma, an age that was considered to record emplacement. In the leucogranites that cut across the biotite +/- cordierite granodiorite, Mrini *et al.* (1992) obtained an Rb-Sr isochron at 295+/- 15 Ma, consistent with the ages of the other leucogranitic rocks elsewhere in the Western Meseta (*e.g.*, the Oulmes leucogranitic pluton dated at 298+/- 6 Ma (Rb/Sr whole-rock); 296 ± 3 Ma

(SHRIMP, U/Pb on zircon) and 308 ± 8 Ma (U/Pb on monazite) (Mrini *et al.*, 1992; Baudin *et al.*, 2001; Fig. 1a)

In summary, both the plutons of the bimodal association and the granodioritic plutons were emplaced in the Jebilet massif at c. 330Ma. Later dykes and stocks of leucogranite were intruded into the granodiorite plutons and the country rocks around 300Ma. The present investigation aims to distinguish, on the basis of Sr and Nd initial isotope ratios at the time of crystallisation, the sources of the diffferent rock-types, and to test if mixing between melts from different sources has occurred. In addition, isotope studies on Variscan magmatism in Morocco are rare (Z. Mrini, unpub. Ph.D. thesis, Univ. Clermont Ferrand, Clermont Ferrand, 1985; Mrini *et al.*, 1992; Gasquet *et al.*, 1992; Ajaji *et al.*, 1998) and this study on the Carboniferous magmatic rocks of the Jebilet massif can be used to place constraints on the genesis of the granitic plutons of the Variscan belt of Morocco.

3. Sampling and analytical methods

Depending on the grain-size, up to 5 Kg weighing samples were collected to represent the range of rock types exposed and to cover the whole area of the bimodal intrusions. Whole-rock geochemical analyses were carried out on samples taken from the different rock types of the main intrusions within the bimodal association, and used with whole-rock geochemical data on the Jebilet peraluminous granodioritic plutons (El Amrani El Hassani, 1996). For Sr-Nd isotopic studies samples were selected **as representative fresh rock, and aim to cover the range of lithological variation within the intrusions.** Samples were selected (1) from mafic-ultramafic rocks of the Kettara mafic-ultramafic intrusion and of the Oled Har, J. Bouzlaf and El Mna composite intrusions, (2) from felsic rocks of the BHD microgranitic lineament and the felsic dykes that cut across the Kettara intrusion, and from felsic-intermediate rocks of the composite intrusions; (3) from cordierite-bearing granodiorites of both the eastern and the western Jebilet plutons, and used with unpublished Sr-Nd isotope data on the ganodiorites and leucogranites (Z. Mrini, unpub. Ph.D. thesis, Univ. Clermont Ferrand, Clermont Ferrand, 1985). **The powder samples were prepared using an agate mortar.**

Whole-rock chemical analyses were performed at the University of Rennes (France) by X-ray fluorescence **spectrometry using a Philips PW 1404 sequential spectrometer**. **Accuracy** for major elements is estimated at 1-3%, except for MnO and P_2O_5 (5%). For trace elements, **accuracy** is of the order of 5% for concentrations lower than 30 ppm, and 3% for concentrations higher than 30 ppm. Selected samples have been analyzed for rare earth elements by ICP MS at the C.R.P.G. (Nancy, France), and **at Laboratoire de Géodynamique des Chaînes Alpines, Grenoble by ICP-MS using a VG PQ2+ spectrometer,** following the procedures described by Barrat *et al.* (1996). **The accuracy is estimated at 5% when chondrite-normalized concentrations are >10 and at 10% when they are lower**. These geochemical data are presented in Table 1.

Sr and/or Nd isotopic compositions were analyzed in thirty samples (Table 2), including different rock types of the bimodal association and one clinopyroxene separated from one gabbro, as well as two samples from each granodioritic pluton. In addition, **Sr isotopes** were analysed in three host rock samples (Sarhlef schists) (Essaifi *et al.*, 2004b). Sr-Nd isotopic analyses were carried out at the University of Rennes (France) using a Finnigan MAT 262 multicollector mass spectrometer. All measured $^{87}Sr/^{86}Sr$ were normalised to $^{86}Sr/^{88}Sr$ = 0.1194, and were measured relative to NBS 987 Sr Standard = 0.71025. The error of $^{87}Sr/^{86}Sr$, including the statistical error obtained during the mass spectrometer run and other error sources such as instrumental reproducibility, is estimated to be ±0.0003. Nd isotopic ratios were normalised to $^{146}Nd/^{144}Nd$ = 0.7219. Additional S**m**-Nd isotopic analyses were performed at Syracuse University (USA) following the procedures described by Samson *et al.*

(1995). During the course of this study, **the NBS 987 Sr standard yielded a mean $^{87}Sr/^{86}Sr$ of 0.710253 at Rennes university,** and the $^{143}Nd/^{144}Nd$ value for the La Jolla standard was 0.511855 at the Syracuse Laboratory **and 0.511858 at Rennes university**. **Even though no samples were run at both laboratories, samples collected from the same intrusion (e.g. MOH1 and 00M04 micrograniticsamples or OH6 and 00M03 gabbroic samples) yielded similar results indicating that** the Sm-Nd isotopic data from the two laboratories are in good agreement.

4. Results

4.a. Secondary alteration

The Variscan magmatic rocks of the Jebilet massif underwent combined effects of hydrothermal alteration and strain (Essaifi *et al.*, 2004a, b; Essaifi & Hibti, 2008; M. K. Ben Salah, unpub. Ph.D. thesis, Univ. Cadi Ayyad, Marrakesh, 1989). Element mobility associated with hydrothermal and deformation processes has resulted in minor geochemical changes in the undeformed rocks comparatively to the deformed ones where most major elements, especially, Na, K and Ca, Mg and Fe, were mobilised. The large-ion lithophile elements (LILE) such as Rb, Ba, Sr, and Zn, Pb and Cu were also mobilised. However, there is no evidence that the high-field strength elements (HFSE), Ti, P, Th, Zr, Nb, Y, or the REE experienced significant mobility during hydrothermal alteration, except inside the fluid channel ways (shear zones). Therefore LILEs and related elements will be avoided for the purposes of petrogenetic discussion.

Table 1 could be placed in the next page

4.b. The ultramafic-mafic rocks of the bimodal association

The mafic-ultramafic rocks include peridotites, gabbros, leucogabbros and dolerites. The majority of these rocks have clearly formed by cumulate processes, producing igneous layering, although some mafic rocks are found in dykes which are more likely to represent magmatic compositions. High Mg, Ni, Co and Cr contents characterise the peridotites due to olivine and spinel accumulation, and high Ca and Al contents in leucogabbros are due to plagioclase accumulation (Fig. 4). The non-cumulate rocks display intermediate Al_2O_3 (≈14-15 wt %), MgO (≈6-9 wt %) and CaO (≈8-11% wt) contents (Table 1). A noticeable silica gap (53-59%) separates the mafic-ultramafic series from the other rock units. The mafic-ultramafic rocks have Mg# (=Mg/Mg+Fe) of 0.62-0.86 in the cumulate rocks and of 0.53-0.7 in the non-cumulate rocks (Fig. 5a). They show a Fe-enriched trend in the FeO*/MgO vs. SiO_2 diagram of Miyashiro (1974) (Fig. 5c) and in FeO* vs. FeO*/MgO (Aarab & Beauchamp, 1987). The mafic-ultramafic rocks have lower Nb/Y (<0.67) than alkaline basalts. In the TiO_2 vs. Zr/P_2O_5 diagram of Winchester and Floyd (1976), the non-cumulate mafic rocks plot in the tholeiitic field (Fig. 6a), which is consistent with the Nb/Y ratios and the Fe-enrichment. The mafic-ultramafic rocks are metaluminous (Fig. 7a). The non-cumulate mafic rocks have higher TiO_2 and $Fe_2O_3^*$ contents than the cumulate rocks, and plot within the field of experimental peridotite melts (Fig. 6b).

The mafic-ultramafic rocks have low but variable ∑REE contents (10 - 62 ppm, 1 - 10 x chondrite), reflecting different abundances and compositions of intercumulus liquids. The lowest concentrations are in the peridotites (∑REE = 11ppm) and the highest in the non-cumulate rocks (fringing microgabbros and doleritic dykes, ∑REE = 51-62ppm) while the leucogabbros have intermediate concentrations (∑REE = 12-17ppm). All the mafic-ultramafic rocks display flat ($(Gd/Yb)_N$=1.06-1.38) heavy rare earth elements (HREE) patterns (Fig. 8a). The cumulate rocks have light-rare-earth elements (LREE) depleted ($(La/Yb)_N$ = 0.4-0.9) patterns reflecting dominance of accumulated crystals over interstitial liquids, while the non-cumulate rocks (microgabbros and dolerites) have flat and linear patterns ($(La/Yb)_N$ = 1.1-1.7). Some mafic-ultramafic rocks display a small Eu anomaly, either positive (Eu/ Eu*= 0.9-1.2) related to plagioclase accumulation or negative (Eu/ Eu*= 0.65-0.9) related to olivine accumulation. All the analysed Jebilet mafic-ultramafic rocks have similar chondrite-normalised HREE patterns, suggesting that they were derived from a common mantle source.

In the primitive mantle-normalised spiderdiagrams (Fig. 8d), the non-cumulate mafic rocks are characterised by flat HFSE patterns and lack the negative Nb anomaly that might be expected in calc-alkaline magmas. The cumulate samples have generally lower HFSE and REE contents than the non-cumulates, reflecting the incompatibility of these elements in the main cumulus minerals, and show positive or negative Sr anomalies due respectively to plagioclase accumulation in leucogabbros and olivine accumulation in peridotites (Fig. 8d). The LILE are generally enriched relative to the REE and HFSE; a feature that can be either related to aqueous fluid involvement (Rollinson, 1993, p. 146) or a characteristic of the source rocks.

The Sr isotopic compositions of the isotropic gabbros, both cumulate and non-cumulate, are variable. Initial $^{87}Sr/^{86}Sr$ calculated at 330 Ma lie in the range 0.7037-0.7087, and the intercumulus clinopyroxene measured on a mineral separate has an initial $^{87}Sr/^{86}Sr$ ratio of 0.7045 (Table 2). The $^{147}Sm/^{144}Nd$ are between 0.17 and 0.3 and the initial $^{143}Nd/^{144}Nd$, calculated at 330Ma, range from 0.51238 to 0.51265 (Table 2). The corresponding $\varepsilon Nd_{(330)}$ values vary from +8.7 to +2.5 (Fig. 9). εNd generally increases with increasing Mg# (Fig. 10).

4.c. The microgranites and quartz-diorites of the bimodal association

The microgranites of the bimodal association are highly differentiated with SiO_2 contents ranging from 70 to 80%. The abundances of immobile elements (Th, Nb, P, Zr, Ti, Y and

REE) do not fluctuate significantly between samples (Fig. 8e), with low TiO_2 and P_2O_5 contents, respectively in the ranges 0.2-0.5% and 0.03-0.06%, except in the Oled Har microgranites where P_2O_5 content reaches 0.25% (Fig. 4). The microgranites have high Zr abundances, between 256 and 380ppm, except in the El Mna composite intrusion where the Zr content reaches 839ppm (Fig. 4). Nb and Th contents are respectively in the ranges 17-23ppm and 29-39ppm, except in the Jbel Bouzlaf composite intrusion where Th content is as low as 17ppm. Ga and Y contents are in the ranges 15-23ppm and 57-115ppm respectively. The least altered granophyric microgranites, preserved in the outer parts of the BHD intrusions where deformation is heterogeneous, have relatively high K_2O contents (Fig. 5b). They are metaluminous to weakly peraluminous (Fig. 7a) and show characteristics of A-type or ferroan granitoids (i) petrographically, they contain Fe-rich biotite, hastingsite and fluorite; (ii) geochemically, their Mg and Ca contents are low (MgO<0.5%, CaO<2%), total alkali contents are high (6-8%), and their Fe/Mg ratio is high (FeO/(FeO+MgO)>0.8; Fig. 11a); (iii) they have relatively high zircon saturation temperatures (850-900°C, Fig. 7b, Table 1), similar to temperatures based on zircon typology (850-900°C, Essaifi *et al.*, 2003), and on amphibole geothermometry (Holland & Blundy, 1994; Essaifi, 1995). There is no evidence for inherited zircon because separates obtained for previous geochronological studies show euhedral, transparent and colourless magmatic zircons that lack internal structures or visible cores (Essaifi *et al.*, 2003). We therefore conclude that such temperatures reflect the temperature conditions during melting; indicating that the A-type microgranites represent high-temperature granitic melts. Transformation by loss of K and gain in Na and Ca resulted in moderately high total alkalis in the Jebilet microgranites (Essaifi *et al.*, 2004a). The microgranites have relatively high Ga/Al (2.3-3.3) and plot within the A-type compositional field of Whalen *et al.* (1987), and especially within the A_2-type granitoid field of Eby (1992)

(Fig. 11b-c). **This is also confirmed by the classification scheme of Frost *et al.* (2001) using the diagram FeO*/(FeO*+MgO) vs. SiO_2 (Fig. 11a)**.

The granophyric microgranites have relatively high REE concentrations (∑REE = 288-386), the concentrations of those in the BHD felsic lineament being identical to those of the felsic rocks of the composite intrusions (Oled Har, El Mna, J. Bouzlaf). They are characterised by uniform patterns (Fig. 8b), with a moderate LREE to HREE fractionation ($(La/Yb)_N$ = 3.6-7.1, $(La/Sm)_N$ = 2.5-3.2)), a constant negative Eu anomaly (Eu/Eu* = 0.3-0.4) and gently sloping HREE chondrite-normalised patterns $(Gd/Yb)_N$ = 1-1.7). In a primitive mantle-normalised trace element plot, the microgranites show an overall enriched pattern except for depletion in Sr, P, Eu and Ti (Fig. 8e). In addition, Nb shows a significantly negative anomaly relative to the neighbouring elements ($(Nb/La)_N$=0.3-0.4).

Chemical compositions of the few intermediate rocks (quartz-diorites) present in the composite intrusions are variable. The SiO_2 content varies between 59 and 69% and Fe_2O_3* between 3 and 10% (Fig. 4). In the El Mna composite intrusion, evolution from mafic-ultramafic rocks to felsic rocks is accompanied by Fe, Mn and P enrichments in the intermediate rocks (sample EM7, Table 1). Such enrichments are, however, absent in the Oled Har and Jebel Bouzlaf composite intrusions (samples OH4 and MBZN5, respectively). The quartz-diorites have contents of immobile elements similar to those in the felsic rocks, except Th and Nb contents that are lower and reach 8 and 10 ppm, respectively (sample EM7, Table 1). They have high Zr contents between 216 and 590 ppm (Fig. 4). The ranges of Ga and Y are 21-25ppm and 42-99ppm respectively. The quartz-diorites plot in the same alkaline fields as the granophyric microgranites (Fig. 11b-c).

The initial Sr isotopic ratios of the granophyric microgranites of central Jebilet range from 0.7079 (0.7073 in the quartz-diorite of El Mna intrusion) to 0.7119. The $^{147}Sm/^{144}Nd$ are between 0.13 and 0.15 and the initial $^{143}Nd/^{144}Nd$, calculated at 330Ma, range from 0.51189 to

0.51218. The corresponding $\varepsilon Nd_{(330)}$ values vary from -0.6 to -6.3 (Fig. 9). The isotopic range is more restricted when the intrusions are considered separately. $\varepsilon Nd_{(330)}$ values are (i) -6.3 and -6.2 in the microgranites of the Oled Har intrusion, (ii) between -2.6 and -3 in the BHD microgranitic intrusions, (iii) -0.6 and -0.7 in the felsic-intermediate rocks of El Mna and Jbel Bouzlaf composite intrusions. **These results reveal a spatial variation in the microgranites characterised by an increase in the $\varepsilon Nd_{(330)}$ values westwards**.

Table 2 could be placed here

4.d. The cordierite-bearing granodiorites and associated leucogranites

The cordierite-bearing granodiorites form differentiated products of a calc-alkaline plutonic suite (Fig. 5b). The plutons also include monzogranites and tonalitic to dioritic magmatic enclaves (El Amrani El Hassani, 1996; Gasquet *et al.*, 1996). They have intermediate to acidic compositions (SiO_2 = 64 - 76%), the most differentiated pluton being the central Jebilet granodiorite. They form continuous and regular trends, distinct from those of the microgranites (Fig. 4). Their biotite compositions correspond to those of calc-alkaline granitic magmas (El Amrani El Hassani, 1996; Gasquet *et al.*, 1996), but the systematic presence of magmatic cordierite in the plutons indicates the peraluminous character of the magma, which is also indicated by A/CNK > 1 (Fig. 7a) and a normative corundum content of 1.7-3.2% (El Amrani El Hassani, 1996; Gasquet *et al.*, 1996).

The cordierite-bearing granodioritic plutons show significant negative anomalies in Sr, Zr and Ti (Fig. 8f) and moderate negative anomalies in P and Eu. They have relatively low zircon saturation temperatures (700-800 °C, Fig. 7b, Table 1), similar to temperatures based on zircon typology and biotite geothermometry (El Amrani El Hassani, 1996). They have intermediate REE abundances (144-207 ppm); the contents in the central Jebilet pluton are identical to those of the eastern Jebilet pluton (El Amrani El Hassani, 1996). They are characterised by uniform REE patterns (Fig. 8c) with a slight to moderate LREE to HREE fractionation ($(La/Yb)_N$ = 4.56-6.98, $(La/Sm)_N$ = 2.93-3.34)), a moderate negative Eu anomaly (Eu/Eu* = 0.32-0.66) and flat to gently sloping HREE chondrite normalised patterns ($(Gd/Yb)_N$ = 0.97-1.29). The leucogranites that cut across the granodiorites are highly differentiated (75<SiO_2<79%) and strongly peraluminous (A/CNK >1, Fig. 7a). They have very low contents of CaO (<0.5%), Fe_2O_3* (<1.3%) and MgO (<0.2%) and higher Co contents than the microgranites (Fig. 4).

In the granodioritic plutons and their magmatic enclaves, the initial Sr isotopic ratios, calculated at 330 Ma, vary largely in the range 0.704-0.7108 while the initial Nd isotopic ratios range from 0.51186 to 0.51242 (Table 2). The corresponding $\varepsilon Nd_{(330)}$ values vary from -6.7 to -4.8 in the cordierite-bearing granodiorites, whilst an $\varepsilon Nd_{(330)}$ of +4.1 is found in a mafic microgranular enclave of dioritic composition (Fig. 9). The leucogranites have the highest initial $^{87}Sr/^{86}Sr$ isotopic ratios (0.7117-0.7177) and low $\varepsilon Nd_{(300)}$ values with the lowest $\varepsilon Nd_{(300)}$ value (-7.2) observed in the Jebilet Carboniferous magmatic rocks.

4.e. The host schist series

The country rocks of the Jebilet magmatism are predominantly metapelites derived from Middle to Upper Visean shales deposited in anoxic platform (Beauchamp, 1984) and are affected by a very low to low-grade metamorphism contemporaneous with a post-Visean shortening (Huvelin, 1977). **Their geochemical data suggest derivation from a continental magmatic arc (Moreno et al., 2008). In the spiderdiagram of figure 12, a representative sample of Sarhlef schists collected by composite sampling is compared to greywackes from passive-margin settings and active-margin settings, after Floyd (1991). A negative**

Sr anomaly, a positive V, Cr, Ni anomaly, a negative Ta-Nb anomaly and slight enrichments in Ti, Yb and LREE are observed in the Sarhlef schists relatively to the upper crust. There is a general correspondence to the continental arc and active-margin tectonic environment, but the presence of a negative Sr anomaly is similar to the passive-margin setting. Sr isotope analysis has been conducted on three samples collected by composite sampling (Essaifi *et al.*, 2004b). Their $^{87}Sr/^{86}Sr$ values at the time of intrusion of the bimodal magmatic association and the granodioritic plutons (330 Ma) vary between 0.7077 and 0.7121 (Fig. 9).

5. Discussion

5.a. Potential magmatic processes

In situ fractional crystallisation (FC) clearly played a major role in the development of the ultramafic-mafic rocks as indicated by mineral layering, cumulate textures, major and trace element geochemistry (e.g. Eu anomalies). However, field relationships, geochemistry and Sr and Nd isotopic compositions allow us to recognize that other petrogenetic processes, such as crustal assimilation, magma mixing, and hydrothermal alteration were also operative in the formation of the Jebilet plutons.

Field relationships provide evidence for magma mixing and mingling (dioritic zones and enclaves in the plutons); incorporation of crustal material (crustal xenoliths in the granodiorites); and metasomatic alteration. As far as possible, samples for geochemical and isotopic analysis were selected from areas that had not been affected by significant metasomatism, and these thus preserve a record of other petrogenetic processes. If fractional crystallisation were the dominant process by which these magmas evolved, little change would be expected in some incompatible element ratios (e.g. La/Nb, Zr/Nb) or in isotopic ratios across the igneous suite. The wide variation in these ratios clearly indicates that magmas were derived from more than one source.

The Carboniferous Jebilet magmatic rocks show large variations in both initial Sr isotopic ratios and Nd values, which display a broad inverse correlation in the Nd vs. Sr_i space (Fig. 9). Since the whole-rock Sm-Nd system is more resistant to late stage low grade perturbations than the Rb-Sr system, this indicates that the scatter of whole-rock Rb-Sr data is not solely related to post-magmatic perturbations but reflects complex petrogenesis. In the mafic-ultramafic rocks, increasing degrees of differentiation (monitored by the Mg#, Fig. 10) are associated with increasing amounts of crustal components (lower εNd values with decreasing Mg#). Such a trend is consistent with mixing between mantle-derived and crust-derived magmas or an assimilation and fractional crystallisation (AFC) process (DePaolo, 1981b). **In the granodioritic samples and the mafic rocks there is a negative correlation between Yb contents and the size of the Eu-anomaly indicating that feldspar fractionation contributes to the size of the negative Eu-anomaly in the mafic rocks and the granodiorites. There is however no correlation of Yb contents with the size of the negative Eu-anomaly in the microgranites. Thus the Eu-anomaly in the microgranites is not due to fractional crystallisation of feldspar but more likely it is a feature of the source rocks in which plagioclase was partly a residual phase.**

Contamination of the microgranites during ascent and emplacement seems probable since they share the same initial isotopic ratios with the host schists (0.707-0.712). However simple contamination is unlikely in the light of the Nd concentration. The microgranites have higher Nd concentrations (50.4-65.47 ppm) than the metasedimentary rocks (14.4-41.5 ppm; Belkabir *et al.*, 2008; Essaifi, unpublished data) and the granodiorites and leucogranites (4.52-48.14 ppm) (Fig. 13). Simple contamination would require that the host schists provide an unacceptably high amount

of the bulk Nd. In simple crustal assimilation models, the size of Nb anomaly and concentration of elements most affected by contamination (Ba, Rb, K, LREE, Sr; Thompson *et al.*, 1982) are expected to increase with progressively more negative $\varepsilon Nd_{(T)}$ values. These relationships are not observed among the microgranites (Fig. 8e). Hence, the Nb negative anomaly in the microgranites is difficult to explain by AFC processes; rather it is a characteristic of the source rocks, similar to that of subduction-related magmas. Xenoliths and xenocrysts from the country rocks are widespread in the granodioritic plutons but are absent from the A-type microgranites, suggesting that chemical exchanges between the microgranites and country rocks are of limited extend. Furthermore, preservation of the different Nd isotopic signatures in the different microgranitic intrusions implies that different batches of magma were produced from different sources or mixtures of different sources. It is therefore suggested that distribution of data points in figure 13 originates through mixing of different end-members rather than by simple contamination processes. Such end-members are discussed in more detail below.

5.b. Inferences on mantle and crustal sources

The mafic-ultramafic rocks have the most primitive isotopic signatures with the lowest $(^{87}Sr/^{86}Sr)_i$ and highest εNd_i values (Fig. 9), whereas the leucogranites and some microgranites are most evolved with the highest $(^{87}Sr/^{86}Sr)_i$ and lowest εNd_i values; the other microgranites and the quartz-diorites on one hand, the granodiorites and their microgranular enclaves on the other hand, form an intermediate group between the mafic-ultramafic rocks and the leucogranites, suggesting a hybrid origin.

5.b.1. Origin of the mafic-ultramafic rocks

Despite their large variations, the available initial εNd values (+8.7 to +2.5) and initial $^{87}Sr/^{86}Sr$ ratios (0.7037 to 0.7087) support a mantle-derived origin for the mafic-ultramafic series. Although many mantle reservoirs have been proposed (e.g. Rollinson, 1993, p. 233), major possible sources are the sub-continental lithospheric mantle, the mantle wedge above a subduction zone, or the asthenospheric mantle. Some fine-grained mafic rocks forming dykes or chilled margins in some of the intrusions may be considered to represent near-liquid compositions. These mafic rocks have consistent, flat trace element and REE patterns, in contrast to the cumulate samples which have more variable trace element compositions. However, even these rocks have rather variable isotopic compositions, suggesting that they have fractionated from slightly or significantly different batches of basic magma. The composition of the source region and parent magma of the mafic-ultramafic series can be approached from the least contaminated samples in terms of Sr-Nd isotopes. The GSK sample is a fine-grained troctolite dyke that has the most primitive isotopic signature currently recorded in the Jebilet massif [$\varepsilon Nd_i = +8.7$ and $(^{87}Sr/^{86}Sr)_i = 0.7037$, Nd=4.68 ppm, Sr = 65 ppm]. This rapidly-chilled dyke may represent a melt with a pristine asthenospheric mantle heritage and hence furnish a reliable estimate of the Sr and Nd isotopic composition of the mantle-derived suite. **Its high Mg# (0.7) and MgO as well as compatible element contents suggest that it represents a primary or near-primary melt**. This is consistent with the flat to LREE depleted patterns of the non-cumulate mafic rocks (Fig. 8a), patterns that are similar to those of N-MORB. These non-cumulate rocks have high TiO_2 contents and plot within the field defined by experimental melts of fertile peridotites (Fig. 6b), suggesting that they were most probably derived from fertile asthenosphere. **However instrumental neutron activation analysis (F. Kharbouch, unpub. Ph.D. thesis, Univ. Bretagne occidentale, Brest, 1994) revealed that some mafic rocks of the bimodal association**

display geochemical features implying that the asthenospheric mantle was affected by subduction processes. These rocks are relatively enriched in LILE and depleted in HFSE with Nb-Ta negative anomalies. Their Nb/U (14-56) and Th/U ratios (1.9-5.19) can be lower than those of MORB and OIB. Such geochemical features cannot be attributed solely to crustal contamination because Th/U ratios of crustal rocks are high (~5.0) and crustal assimilation will elevate Th/U ratios higher than those of MORB (~3.0) and OIB (~3.4) (Jiang *et al*., 2009). Th/U ratios of the slab-released hydrous fluid are low because U, relatively to Th, is preferentially transported in the aqueous fluid, from the subducted slab to the mantle wedge (Keppler, 1996; Ayers, 1998). Based on immobile-discrimination diagrams as the Th-Hf-Ta diagram of Wood *et al*. (1980), the Jebilet mafic rocks include both MORB-like and destructive plate-margin-like basaltic compositions (Fig. 14a). Such a coexistence of MORB-like and Arc-like tholeiitic basalts has also been described in other bimodal association involving A_2-type rhyolites and tholeiitic basalts (e.g. the Topsails igneous suite in the Newfoundland Appalachians, Whalen *et al*., 2006). For this reason we believe that although contamination has played a role in modifying their composition, mafic rocks of the Jebilet massif are thought to be derived from different mantle sources, a depleted MORB mantle and a mantle wedge above a subduction zone.

Gasquet *et al*. (1992) showed that mafic rocks (gabbros and diorites) from the nearby Variscan Tichka plutonic complex (Fig. 1a) are derived from an upper mantle source, and that this high temperature magma provided the heat for the production of granitoid magmas by partial melting of the continental crust. **On the Nd-Sr isotope diagram (Fig. 9), the Tichka plutonic rocks plot within the mantle array as defined by uncontaminated oceanic basalts, whereas most of the Jebilet mafic rocks plot to the right of this field. Clearly the Nd-Sr isotope data of the Jebilet mafic rocks could be accounted for simply by partial**

melting of a depleted asthenospheric mantle wedge (MORB source mantle) enriched in radiogenic Sr by slab derived fluids. The fact that Th/Yb ratios are displaced towards higher values in the Th/Yb vs. Ta/Yb diagram (Fig. 14b) provides strong evidence for involvement of such slab-derived fluids in the genesis of the Jebilet mafic rocks.

5.b.2. Origin of the microgranites

The Jebilet granophyric microgranites show geological and geochemical features that are characteristic of A-type or **ferroan granites** according to criteria proposed by several authors (e.g., Collins *et al.*, 1982; Whalen *et al.*, 1987; Eby, 1992; **Frost *et al.*, 2001**) (1) they were intruded to very high levels in the crust as indicated by granophyric intergrowths along with comagmatic sub-volcanics emplaced at the same structural level, (2) they contain interstitial Fe and Cl-rich biotite, hastingsite and fluorite, (3) their Mg and Ca contents are low and their REE (except Eu) and HFSE contents are high (Fig. 8b, e), (4) they also have high magmatic temperatures (up to 900°C, Fig. 7b) and their Fe/Mg and Ga/Al ratios are high (Fig. 11a-b). High Rb/Nb and Y/Nb ratios (Fig. 11c) further suggest that these granites belong to the A_2 group of Eby (1992); a group of alkaline granitoids derived from continental crust or underplated crust that has been through a cycle of continent-continent collision or the waning stages of arc magmatism, whereas the A_1-type granites emplaced in continental rifts or during intraplate magmatism and represent differentiates of magmas derived from OIB-like sources (Eby, 1992).

The A-type magmas are regarded as differentiation products of mantle-derived melts through extensive fractional crystallisation (e.g. Turner *et al.*, 1992; Bonin, 1996; Litvinovsky *et al.*, 2002; Mushkin *et al.*, 2003), or as partial melts of specific crustal protoliths, either a granulitic residue from which a granitic melt was previously extracted (Collins *et al.*, 1982; Whalen *et al.*, 1987; Creaser *et al.*, 1991; Clemens, 1986), a charnockitic rock (Landenberger & Collins, 1996), a hornblende-bearing granitoid (Patiño Douce, 1997), or a granulitic metasedimentary rock (Huang *et al.*, 2011). They could also result from hybridisation between anatectic granitic and mantle-derived mafic magmas (Bédard, 1990; Kerr & Fryer, 1993; Mingram *et al.*, 2000; Yang *et al.*, 2006), coupled with fractionation processes (Barker *et al.*, 1976; Wickham *et al.*, 1996).

The presence of a ”Daly gap” between mafic-ultramafic rocks and the micrograntes and some crust-like geochemical and isotopic features argues against a simple magma differentiation model. Th concentrations in the Jebilet microgranites (20 – 40ppm; Table 1) are higher than in the oceanic plagiogranites (Th < 5ppm; Pearce *et al.*, 1984), suggesting that these microgranites do not result from the differentiation of the penecontemporaneous tholeiitic basalts (Th≤2ppm). For the same SiO_2 content, the microgranites of Central Jebilet are especially poor in Ti and Fe compared to the granophyres associated with well known layered tholeiitic intrusions (e.g. McBirney, 1989; Turner *et al.*, 1992). In any case, the Sr initial isotopic ratios and the εNd values of the granophyric microgranites are distinct from those of the associated gabbroic rocks (Fig. 9) and leave no doubt that the microgranites did not form simply by extensive fractional crystallisation from the coeval mantle-derived mafic magmas. **Therefore their origin should involve continental crust, either lower or upper crust**.

High REE contents but moderate $\varepsilon Nd_{(330)}$ values imply that the sources are not strongly evolved and preclude the derivation of the A-type microgranites from granulitic metasedimentary rocks. The high HREE (Yb> 6.22 ppm, up to 10.5 ppm) and Y (> 69 ppm, up to 115 ppm) contents and flat to gently sloping HREE patterns (Fig. 8b) of the Jebilet microgranites preclude garnet as a residual phase, which implies low pressure (< 7 Kb, Patiño Douce, 1997). Based on comparisons with experimentally produced melts from a variety of crustal lithologies (Holloway & Burnham, 1972; Helz, 1976; Spulber & Rutherford, 1983; Beard & Lofgren, 1991; Skjerlie & Johnson, 1993; Patiño Douce, 1997), tonalitic sources are found to be the most consistent with observed compositions of these granophyric microgranites. Melting experiments of Patiño Douce (1997) demonstrated that dehydration melting of hornblende-bearing granitoids in the shallow crust (P ≤ 4 kbar, at the depths of 15 km or less) is a likely origin for high-silica metaluminous A-type granites. At 4 kbar and a melt fraction of 20 to 40%, plagioclase and clinopyroxene are the dominant residual phases of dehydration melting of hornblende-bearing granitoids (Patiño Douce, 1997). **Good matches between the composition of the microgranites and the experimentally produced melts from tonalitic sources lend support to a crustal anatectic origin**.

The Jebilet granophyric microgranites have Proterozoic T_{DM} ages (1.91-1.36 Ga) suggesting that an older crustal component exists in these Carboniferous granitoids. Such old crust, which crops out under the Palaeozoic cover in the Anti-Atlas inliers and is recognised by gravity data under the Palaeozoic formations of the Jebilet massif (Bernardin *et al.*, 1988), has been dated in granulitic enclaves of the Triassic lamprophyre dykes that cross cut the Jebilet massif (Dostal *et al.*, 2005) and in the nearby Rehamna massif (Baudin *et al.*, 2002). **The microgranitic samples from the Oled Har intrusion have the lowest εNd value (-6.3) of the microgranites. Their TDM ages (~1.9 Ga) point to the Eburnean basement (~2 Ga) while the other microgranites have lower TDM ages (1350-1550 Ma) that seemingly require a mafic or juvenile (mantle) component. The coeval association of the microgranites with mafic magmas, the presence of net-veining structures and mafic enclaves within the microgranites suggest interaction between felsic and mafic magmas. In the εNd vs. Sr_i space (Fig. 9), the microgranites are characterized by higher initial $^{187/}Sr/^{186}Sr$ ratios and lower initial εNd values than the mafic rocks. Their field appears to extrapolate back to that of the associated mafic rocks, suggesting some form of mixing process, but this broad inverse correlation cannot be fitted by a single curve diagnostic of a simple two-component mixing. The microgranites trend could represent variable**

degree of mixing between a mantle source variably enriched by slab-derived fluids and partial melts of the Eburnean metamorphic basement. This is consistent with the fact that the microgranites show an increase in the mantle contribution from east to west, suggesting the existence of independent reservoirs, in which magmas batches evolved independently by fractional crystallisation and magmas mixing processes.

Curved evolutions for some elements (Ti, Fe, P, V, Zr) in the bimodal association indicate that mineral fractionation was a main petrogenetic process (Fig. 4). Such evolutions are observed in the El Mna intrusion where the quartz-diorite and the microgranite have a same initial εNd value (-0.6), consistent with fractional crystallisation. The εNd value (+2.5) of the associated mafic rock requires assimilation of continental crust in order to produce the Nd isotopic composition of the quartz-diorite and microgranite. Therefore the chemical and Sr-Nd isotopic compositions of some microgranites can be explained by a complex petrogenetic process combining fractional crystallisation and magma mixing between mantle-derived magmas and crust-derived magmas (represented by the Oled Har microgranites). The differences in the isotopic compositions of the microgranites can be related to the heterogeneity of the mantle sources and to variable degree of crustal and mantle contribution.

5.b.3. Origin of the granodiorites and leucogranites

The Jebilet granodioritic plutons are emplaced at high structural levels; they contain biotite, cordierite, and ilmenite; and they are strongly peraluminous. Therefore they can be attributed to the S-type granite group of Chappell & White (1974). Such granites are largely produced by partial melting of metasedimentary rocks. Barbarin (1996) has distinguished two groups among the S-type granites (i) biotite-rich, cordierite-bearing granitoids (CPG-type) and (ii) muscovite-bearing granitoids (MPG-type). The CPG granitoids are suggested to be produced by “dry” anatexis of crustal rocks enhanced by underplating or injection of hot mantle-derived magmas, which can be preserved as microgranular mafic enclaves within the CPG (Barbarin, 1996). As the Jebilet granodioritic plutons contain numerous microgranular mafic enclaves; they can be attributed to the CPG type.

The T_{DM} ages of the granodioritic plutons (1.76 – 0.85 Ga) require a Proterozoic source rock. Their strongly peraluminous signature suggests that the source rocks were mainly metasedimentary rocks rather than meta-igneous rocks. However, the plutons display large variations in Sr-Nd isotopic compositions that may indicate the presence of a mantle-derived component, and the granodiorite plutons contain numerous microgranular mafic enclaves. Therefore, as suggested by Barbarin (1996), these rocks might be derived from anatexis of crustal rocks induced by underplating or injection of hot mantle-derived magmas. The granodioritic plutons have intermediate HREE (2.42 ppm $<$Yb$<$ 4.47 ppm) and Y (21-34 ppm) contents and overall display flat to gently sloping HREE patterns ($(Gd/Yb)_N$ = 1-1.7). Fractionation among the HREE, a common feature of S-type granites (e.g. Bernard-Griffiths, 1985) would indicate the presence of garnet in the residual source, but this feature is lacking in the cordierite-bearing granodiorites of the Jebilet. Therefore, these magmas were more likely produced by relatively low temperature (~750°C) anatexis of pelitic sources induced by injection of basalt magmas in the shallow crust. The produced crustal melts underwent hybridisation with the coeval basalt magmas and assimilation of pelitic metasediments during ascent of the magmas in the crust. The process of wall rock assimilation was documented in the Jebilet granodioritic plutons by the occurrence of inherited metamorphic cordierites, which are partly digested pelitic xenoliths, picked up at 750 °C and 3.5 kbar by the ascending magma (Bouloton, 1992), and therefore representing relics of the assimilated rocks (Fourcade *et al.*, 2001). The large variation in the initial Sr isotopic ratios (0.704-0.7108) and the $\varepsilon Nd_{(330)}$

values (-6.7 to +4.1) in the granodioritic plutons indicates isotopic heterogeneity that results from mixing between crust-derived and mantle-derived magmas (Mrini *et al.*, 1992) and wall-rock assimilation. **The granodiorites define continuous and regular trends in major and trace elements diagrams (Fig. 4). In the εNd vs. Sr_i diagram (Fig. 9), the granodiorites and their microgranular enclaves scatter around a hyperbolic mixing curve between a** crustal end-member corresponding to the mean composition of the protolith from which most of the granites in Morocco were derived (Z. Mrini, unpub. Ph.D. thesis, Univ. Clermont Ferrand, Clermont Ferrand, 1985) and the mantle end-member of the Tichka plutonic complex.

The two mica-leucogranites are strongly peraluminous and can be described as S-type granites of Chappell & White (1974) and muscovite-bearing granitoids (MPG-type) (Barbarin, 1996). The initial Sr isotopic ratio (0.7177) and the $\varepsilon Nd_{(330)}$ value (-7.2) of the Jebilet leucogranites are consistent with direct derivation from crustal sources with a major contribution of aluminous metasedimentary rocks.

5.c. Magma generation/tectonic implications

The question of the heat source required for crustal melting during granitoid genesis is a long-debated topic, with i) purely crustal mechanisms involving crustal thickening and total heat supply by decay of radioactive elements (e.g., England & Thompson, 1986) and ii) mantle-crust mechanisms involving heat input from the mantle into the crust in various geodynamic situations: asthenospheric upwelling (hot spots or extension zones), arc genesis, and lithospheric delamination or slab break-off in orogenic zones (e.g., Harris *et al.*, 1986, Bussy *et al.*, 2000, Whalen *et al.*, 2006).

The spatial and temporal association of mafic magmatism with alkaline and calc-alkaline felsic magmatism in the Jebilet massif argues for mafic magma-driven partial melting. Among the geodynamic settings where the mantle is classically implicated, hot spots or extension zones can be ruled out on the basis of regional tectonics. Relationships between deformation, magmatism and metamorphism indicate that emplacement of the granodioritic plutons and the bimodal plutonism in the Jebilet massif, as well as emplacement of the wider Carboniferous plutonic suite in the Moroccan Meseta, was contemporaneous with a syn-tectonic low-pressure regional metamorphism and development of ubiquitous, upright axial plane cleavages, unambiguously indicating horizontal shortening at the orogenic scale (Lagarde *et al.*, 1990). Models involving local lithospheric extension in strike-slip-induced basins (e.g. Mitjavila *et al.*, 1997; Essaifi *et al.*, 2003) are also not sustainable because the lithospheric thinning required to induce asthenospheric melting is much too great to be a result of strike-slip shearing during plate convergence. In central Jebilet, syn-tectonic emplacement of magmatic intrusions is consistent with the regional strain pattern that involves NE-SW extension (Fig. 1b), in parallel to the southern prolongation of the western Meseta shear zone (Piqué *et al.*, 1980; Lagarde & Michard, 1986). The NE-SW extension is accompanied by lateral extrusion of the central Jebilet block and by syn-convergence exhumation of the Proterozoic basement and intermediate P/T metamorphic rocks in the Rehamna massif (Aghzer & Arenas, 1998; Baudin *et al.*, 2002). Such an orogen-parallel extension with exhumation is intimately related to continental collision and occurs even during the early stages of convergence (Seyferth & Henk, 2004).

The Jebilet Carboniferous magmatic rocks were emplaced c. 330 Ma into slightly older Upper Visean (350-333 Ma) marine syntectonic “flysch” metasediments. **The positive V-Cr-Ni-Ti anomalies observed in these sediments (Fig. 12) are indicative of a mafic input, involving oceanic crust, possibly obducted onto the continent during a collision event (Floyd, 1991;**

Totten et al., 2000). Their spiderdiagram, with a general correspondence to the continental arc and active-margin tectonic environment and the presence of a negative Sr anomaly similar to the passive-margin setting, is best described by mixing between a dominant passive-margin source and a sediment from an active margin setting (Totten et al., 2000). In Central Morocco, Carboniferous syntectonic "flysch" and catastrophic sediments were deposited in a compressional retro-foreland basin where interbedded basaltic lavas, doleritic dykes and gabbro sills were emplaced during thrusting (Ben Abbou *et al.*, 2001; Roddaz *et al.*, 2002). In the Guemassa massif at the southern prolongation of the Jebilet massif (Fig.1), basaltic dykes and rhyolites were also emplaced during thrusting. Thus the Moroccan Variscan crust seems to have thickened by extensive sedimentation, volcanism and minor intrusion in the upper crust, with synchronous magmatic underplating and ductile deformation at depth. Such crustal thickening characterizes subduction-related orogens (Lamb *et al.*, 1997). In this context one possible extrusive equivalent of the bimodal association of Central Jebilet is the bimodal basalt-subalkaline/peralkaline rhyolite province of the Southern British Caledonides which is also associated with polymetallic sulphide mineralisation (Leat *et al.*, 1986; Thorpe *et al.*, 1993; Eby, 1992). This association was emplaced within a shallow marine environment in a tectonic setting associated with closure of the Lower Palaeozoic Iapetus Ocean, cessation of oceanic subduction and development of strike-slip tectonism. Because the Moroccan Hercynides are thought to be related to continental subduction (Piqué & Michard, 1989; Piqué *et al.*, 1993; Lagarde, 1989; Roddaz *et al.*, 2002), the bimodal association of central Jebilet can be interpreted as resulting from cessation of continental subduction and development of strike-slip tectonism during collision (Fig. 15).

Possible models leading to generation of mafic magmas and crustal melting in collisional orogens include slab break-off (e.g., Davies & von Blanckenburg, 1995), convective lithospheric erosion (Houseman *et al.*, 1981) and large-scale delamination of the lithosphere (e.g. Nelson, 1992). Taking into account the evolution of magmatism in the Jebilet massif, as well as in the Moroccan Meseta (Mrini *et al.*, 1992; El Hadi *et al.*, 2006), from calc-alkaline granitoids and mafic magmas of mixed origin to leucogranites of a purely crustal origin, and synchronous emplacement of these magmas with regional deformation, convective lithospheric erosion during crustal thickening (Loosveld & Etheridge, 1990) seems more consistent with geochemical and Sr-Nd isotopic constraints. Convective thinning/erosion of the lithospheric mantle induces partial melting of subduction-metasomatised subcontinental lithospheric mantle, producing early potassic magmas and progressing to intra-plate depleted asthenospheric melts over time (Mahéo *et al.*, 2002). Potassic to shoshonitic calc-alkaline I-type granitoids crop out in the eastern Moroccan Meseta where they postdate an early, Eo-Variscan folding phase. According to Ajaji *et al.* (1998), the Tanncherfi intrusive complex, emplaced 344 ± 6 Ma ago, was derived from mantle sources enriched in LILE and LREE by a subduction process. The evolution from continental lithospheric mantle signature in the Tanncherfi intrusive complex to the asthenospheric one in the Jebilet massif, as well as in the Tazekka and Tichka massifs (Chalot-Prat, 1995; Gasquet *et al.*, 1992), reflects a lithosphere being progressively heated from below (Houseman *et al.*, 1981; Nelson, 1992). Progressive replacement of the lithosphere by the asthenosphere results in elevated Moho temperatures and thus favours crustal melting at sequentially shallower levels (Fig. 15). The calc-alkaline granitoids become increasingly crustally contaminated and are succeeded by partial crustal melts (Turner *et al.*, 1999; Wang *et al.*, 2004). According to structural, geochemical and Sr-Nd isotopic data, erosion of the mantle lithosphere (thinning) was initiated during crustal thickening and the induced thermal anomaly was responsible for both magmatism and metamorphism in the Variscan Moroccan Meseta.

6. Conclusion

In the Jebilet massif, the post-Visean crustal shortening was accompanied by an orogen-parallel extension, lithospheric thinning, mantle uplift and progressive melting of the depleted mantle, which produced basaltic magmas. These basalts ascended into the continental crust, including the upper crust, where they formed crustal magma chambers. Temperature elevation due to mantle uplift and basalt emplacement induced crustal anatexis. High temperature (~ 900°C) melting of tonalitic sources produced A_2–type granitoids while at low temperatures (~ 750°C) anatexis of metasediments produced cordierite-bearing granitoids. During this evolution, contamination/mixing occurred between mantle-derived magmas and crustal melts, contributing to the large variations of $\varepsilon Nd_{(330)}$ and $(^{87}Sr/^{86}Sr)_i$ values observed in both the cordierite-bearing granitoids and the A_2-type microgranites. Further contamination occurred by assimilation of country rocks during ascent of the magmas to high crustal levels.

The Jebilet magmatism is an example of granitoid magma production in a complex tectonic setting where plate convergence is interacting with a deep process promoting mantle and crust activation. Structural, geochemical and Sr-Nd isotopic constraints argue for convective thinning/erosion of the lithospheric mantle during thickening. The thermal anomaly induced by the convective thinning of the mantle lithosphere is likely to have brought the heat energy that caused melting of the underlying asthenosphere and coeval production of calc-alkaline and alkaline granitoids, which were followed by production of leucogranites.

Acknowledgements

Constructive comments and suggestions by Mike Fowler and another anonymous reviewer, which have greatly improved presentation of data and discussion, are highly appreciated, although some wishes could unfortunately not be fulfilled. We wish to thank J. A. Barrat and G. Gruau from Geosciences Rennes for providing some of the Sr-Nd isotope and REE data used in this study. Sm-Nd isotopes analysed at Syracuse University were conducted during a post doctoral research grant provided by the Fulbright program. We thank S. Fourcade for a review of an early version of this paper. This work is a contribution to the project URAC 43.

Declaration of interest

None

References

AARAB, E. M. & BEAUCHAMP, J. 1987. Le magmatisme carbonifère pré-orogénique des Jebilet centrales (Maroc). Précisions pétrographiques et sédimentaires. Implications géodynamiques. *Comptes Rendus de l'Académie des Sciences, Paris* **304**, 169-174.

AGHZER, A. M. & ARENAS, R. 1998. Evolution métamorphique des métapélites du Massif hercynien des Rehamna (Maroc): implications tectonothermales. *Journal of African Earth Sciences* **27**, 87-106.

AYERS, J. 1998. Trace element modelling of aqueous fluid–peridotite interaction in the mantle wedge of subduction zones. *Contributions to Mineralogy and Petrology* 132, 390–404.

AJAJI, T., WEIS, D. GIRET, A. & BOUABDELLAH, M. 1998. Coeval potassic and sodic calc-alkaline series in the postcollisional Variscan Tanncherfi intrusive complex, north-eastern Morocco: Geochemical, isotopic and geochronological evidence. *Lithos* **45**, 371-393.

BARBARIN, B. 1996. Genesis of the two main types of peraluminous granitoids. *Geology* **24**, 295-298.

BARKER, F., WONES, D. R., SHARP, W. N. & DESBOROUGH, G. A. 1975. The Pikes Peak Batholith, Colorado Front Range, and a model for the origin of the gabbro-anorthosite-syenite potassic granite suite. *Precambrian Research* **2**, 97-160.

BARRAT, J. A., KELLER, F., AMOSSÉ, J., TAYLOR, R. N., NESBITT, R. W. & HIRATA, T. (1996). Determination of rare earth elements in sixteen silicate reference samples by ICP-MS after Tm addition and ion exchange separation. *Geostandards Newsletter* **20**, 133-140.

BAUDIN, T., CHEVREMONT, P., RAZIN, P., THIEBLEMONT, D., RACHDI, H., ROGER, J., BENHAOURCH, R. & WINCKEL, A. 2001. Carte Géologique du Maroc au 1/50 000. Feuille d'Oulmès. *Notes et Mémoires Service Géologique Maroc* **410 bis,** 1-77.

BAUDIN. T., CHEVREMONT, P., RAZIN, P., YOUBI, N., ANDRIES, D., HOEPFFNER, C., THIEBLEMONT, D., CHIHANI, E. M. & TEGYEY, M. 2002. Carte géologique du Maroc au 1/50 000, feuille de Skhour des Rehamna, Mémoire explicatif. *Notes et Mémoires Service Géologique Maroc* **435**, 1-114.

BEARD, J. S. & LOFGREN, G. E. 1991. Dehydration melting and water-saturated melting of basaltic and andesitic greenstones and amphibolites at 1, 3, and 6.9 kb. *Journal of Petrology* **32**, 365-104.

BEAUCHAMP, J. 1984. Le carbonifére inférieur des Jebilet et de l'Atlas de Marrakech (Maroc) : migration et comblement d'un bassin marin. *Bulletin de la Société Géologique de France* **7**, 1025-1032

BEAUCHAMP, J., IZART, A. & PIQUE, A. 1991. Les bassins d'avant pays de la chaîne hercynienne au Carbonifère inférieur. *Canadian Journal of Earth Sciences* **28**, 2024-2041.

BÉDARD, J. 1990. Enclaves from the A-Type Granite of the Mégantic Complex, White Mountain Magma Series- Clues to Granite Magma genesis. *Journal of Geophysical Rsearch* **95**, 17797-17819.

BELKABIR, A., MARCOUX, E., GIBSON. H. LENTZ, D & RZIKI, S. 2008. Geology and wall rock alteration at the Hercynian Draa Sfar Zn–Pb–Cu massive sulphide deposit, Morocco. *Ore Geology Reviews* **33**, 2-306.

BEN ABBOU, M., SOULA, J. C., BRUSSET, S., RODDAZ, M., NTARMOUCHANT, A., DRIOUCH, Y., CHRISTOPHOUL, F., BOUABDELLI, M., MAJESTÉ-MENJOULAS, C., BÉZIAT, D., DEBAT, P. & DÉRAMOND, J. 2001. Contrôle tectonique de la sédimentation dans le système de bassins d'avant-pays de la Meseta marocaine. *Comptes Rendus de l'Académie des Sciences, Paris* **332**, 703-709.

BERNARDIN, C., CORNEE, J. J., CORSINI, M., MAYOL, S., MULLER, J. & TAYEBI, M. 1988, Variations d'épaisseur du Cambrien moyen en Meseta marocaine occidentale: signification géodynamique des données de surface et de subsurface. *Canadian Journal of Earth Sciences* **25**, 2104-2117.

BERNARD-GRIFFITHS, J., PEUCAT, J. J., SHEPPARD, S. M. F. & VIDAL, P. 1985. Petrogenesis of Hercynian leucogranites from the southern Armorican massif: contribution of REE and isotopic Sr, Nd, Pb and O geochemical data to the study of source rock characteristics and ages. *Earth and Planetary Science Letters* **74**, 235–250.

BONIN, B. 1996. A-type granite ring complexes: mantle origin through crustal filters and the anorthosite–rapakivi magmatism connection. In *Petrology and Geochemistry of Magmatic Suites of Rocks in Continental and Oceanic Crusts. A Volume Dedicated to Professor Jean Michot* (ed. Demaiffe, D.), pp. 201-218. Université Libre de Bruxelles, Royal Museum for Central Africa, Tervuren.

BORDONARO, M., GAILLET, J. L. & MICHARD, A. 1979. Le géosynclinal carbonifère sud-mésetien dans les Jebilet (Maroc) : une corrélation avec la province pyriteuse du Sud de l'Espagne. *Comptes Rendus de l'Académie des Sciences, Paris* **288**, 1371-1374.

BOULOTON, J. 1992. Mise en évidence de cordiérite héritée des terrains traversés dans le pluton granitique des Oulad Ouaslam (Jebilet, Maroc). *Canadian Journal of Earth Sciences* **29**, 658-668.

BOULOTON, J. & GASQUET, D. 1995. Melting and undercooled crystallisation of felsic xenoliths from minor intrusions (Jebilet massif, Morocco). *Lithos* **35**, 201-219.

BOUMMANE, M. H. & OLIVIER, PH. 2007. The Oulad Ouaslam Variscan granitic pluton (Jebilet Massif, Southwestern Moroccan Meseta): a forcibly emplaced laccolithic intrusion characterized by its magnetic and magmatic fabrics *Journal of African Earth Sciences* **47**, 49–61.

BUSSY, F., HERNANDEZ, J. & VON RAUMER, J. 2000. Bimodal magmatism as a consequence of the post-collisional readjustment of the thickened Variscan continental lithosphere (Aiguilles Rouges - Mont Blanc Massifs, Western Alps). *Transactions of the Royal Society of Edinburgh: Earth Sciences* **91**, 221-233.

CHALOT-PRAT, F. 1995. Genesis of rhyolitic ignimbrites and lavas from distinct sources at a deep crustal level: field, petrographic, chemical and isotopic-Sr, Nd constraints in the Tazekka volcanic complex, Eastern Morocco. *Lithos* **36**, 29-49.

CHAPPELL, B. W. & WHITE, A. J. R. 1974. Two contrasting granite types. *Pacific Geology* **8**, 173-174.

CLEMENS, J. D. 1986. Origin of an A-type granite: Experimental constraints. *American Mineralogist* **71**, 317-324.

COLLINS, W. J., BEAMS, S. D., WHITE, A. J. R. & CHAPPELL, B. W. 1982. Nature and origin of A type granites with particular reference to Southern Australia. *Contributions to Mineralogy and Petrology* **80**, 189-200.

CREASER, R. A., PRICE, R. C. & WORMALD, R. J. 1991. A-type granites revisited: Assessment of a residual-source model. *Geology* **19**, 163-166.

DAVIES, J. H. & VON BLANCKENBURG, F. 1995. Slab break-off: a model of lithosphere detachment and its test in the magmatism and deformation of collisional orogens. *Earth and Planetary Science Letters* **129**, 85-102.

DEPAOLO, D. 1981a. Neodymium isotopes in the Colorado Front Range and crust-mantle evolution in the Proterozoic. *Nature* **291**, 193-196.

DEPAOLO, D.J., 1981b. Trace element and isotopic effects of combined wallrock assimilation and fractional crystallization. *Earth and Planetary Science Letters* **53**, 189–202.

DIOT, H. & BOUCHEZ, J. L., 1989. Les granitoïdes hercyniens de la haute Moulouya : leur structure primaire déduite de l'ASM. Indications sur leur mise en place. *Bulletin de la Société Géologique de France* **4**, 705-71.

DOSTAL, J., KEPPIE, J. D., HAMILTON, M. A., AARAB, E. M., LEFORT, J. P. & MURPHY, J. B. 2005. Crustal xenoliths in Triassic lamprophyre dykes in western Morocco: tectonic implications for Rheic Ocean suture. *Geological Magazine* **142**, 159-172.

EBY, N. G. 1992. Chemical subdivision of the A-type granitoids: Petrogenetic and tectonic implications. *Geology* **20**, 641-644.

EL AMRANI EL HASSANI, I. E. 1996. Petrogenèse des granitoïdes peralumineux des Jebilet centrales (Maroc) : approche par l'étude des enclaves. *Bulletin Institut Scientifique Rabat* **20**, 1-23.

EL HADI, H., SIMANCAS CABRERA, F., TAHIRI, A., GONZALEZ LODEIRO, F., AZOR PEREZ, A. & MARTINEZ POYATOS, D. J. 2006. Comparative review of the Variscan granitoids of Morocco and Iberia: proposal of a broad zonation. *Geodinamica Acta* **19**, 103-116.

ENGLAND, P. C. & THOMPSON, A. 1986. Some thermal and tectonic models for crustal melting in continental collision zones. In *Collision tectonics* (Eds. M.P. Coward & A.C. Ries), pp. 83-94. Geological Society of London, Special Publications no. 19.

ESSAIFI, A. 1995. Relations entre magmatisme-déformation et altération hydrothermale: l'exemple des Jebilet centrales (Hercynien, Maroc). *Mémoires Géosciences Rennes*, **66**, 1-340.

ESSAIFI, A., LAGARDE, J. L. & CAPDEVILA, R. 2001. Deformation and displacement from shear zone patterns in the Variscan upper crust, Jebilet, Morocco. *Journal of African Earth Sciences* **32**, 335-350.

ESSAIFI, A., POTREL, A., CAPDEVILA, R. & LAGARDE, J. L. 2003. U-Pb dating: emplacement age of the bimodal magmatism of central Jebilet (Variscan Belt, Morocco). Geodynamic implications. *Comptes Rendus Géoscience* **335**, 193-203.

ESSAIFI, A., CAPDEVILA, R. & LAGARDE, J. L. 2004a. Metasomatic Trondhjemites and Tonalites: Examples in Central Jebilet Variscan (Morocco). *Journal of African Earth Sciences* **39**, 369-374

ESSAIFI, A., CAPDEVILA, R., FOURCADE, S., LAGARDE, J. L., BALLEVRE, M. & MARIGNAC, C. 2004b. Hydrothermal alteration, fluid flow and volume change in shear zones: the layered mafic-ultramafic Kettara intrusion (Jebilet massif, Variscan belt, Morocco). *Journal of Metamorphic Geology* **22**, 25-43.

ESSAIFI, A. & HIBTI, M. 2008. The hydrothermal system of Central Jebilet (Variscan Belt, Morocco): a genetic association between bimodal plutonism and massive sulphide deposits. *Journal of African Earth Sciences* **50**,188-203

EVENSEN, N. M., HAMILTON, P. J. & O'NIONS, R. K. 1978. Rare-earth abundances in chondritic meteorites. *Geochimica Cosmochimica Acta* **42**, 1199-1212.

FALLOON, T. J., GREEN, D. H., HATTON, C. J. & HARRIS, K. L. 1988. Anhydrous partial melting of a fertile and depleted peridotite from 2 to 30 kb and application to basalt petrogenesis. *Journal of Petrology* **29**, 1257-1282.

FLOYD, P.A., 1991. Rhenohercynian sandstone chemistry. In *Developments in sedimentary provenance studies* (Eds. A.C. Morton, S.P.Todd & Haughton P.D.W). pp. 173–188. Geological Society of London, Special Publication no. 57.

FOURCADE, S., CAPDEVILA, R., OUABADI, A. & MARTINEAU, F. 2001. The origin and geodynamic significance of the Alpine cordierite-bearing granitoids of northern Algeria. A combined petrological, mineralogical, geochemical and isotopic (O, H, Sr, Nd) study. *Lithos* **57**, 187-216.

FROST, B. R. BARNES, C. G., COLLINS, W. J. ARCULUS, R. J. ELLIS, D. J. & FROST, C. D. 2001. A Geochemical Classification for Granitic Rocks. *Journal of Petrology* **42**, 2033–2048

GASQUET, D., STUSSI, J. M. & NACHIT, H. 1996. Les granitoïdes hercyniens du Maroc dans le cadre de l'évolution géodynamique régionale. *Bulletin de la Société Géologique de France* **167**, 517-528.

GASQUET, D., LETERRIER, J., MRINI, Z. & VIDAL, P. 1992. Petrogenesis of the Variscan Tichka Plutonic Complex, Western High.Atlas, Morocco: trace element and Rb–Sr and Sm–Nd isotopic constraints. *Earth and Planetary Science Letters* **108**, 29-44.

HARRIS, N. B. W., PEARCE, J. A. & TINDLE, A. G. 1986. Geochemical characterization of collision-zone magmatism. In *Collision Tectonics* (Eds. M.P. Coward & A.C. Ries), pp. 67-81. Geological Society of London, Special Publication no. 19.

HELZ, R. T. 1976. Phase relations of basalts in their melting ranges at P = 5 kb. Part II. Melt compositions. *Journal of Petrology* **17**, 139-193.

HOEPFFNER, C., SOULAIMANI, A. & PIQUÉ, A. 2005. The Moroccan Hercynides. *Journal of African Earth Sciences* **43**, 144-165.

HOLLAND, T. & BLUNDY, J. 1994. Non-ideal interactions in calcic amphiboles and their bearing on amphibole–plagioclase thermometry. *Contributions to Mineralogy and Petrology* **116**, 433-447.

HOLLOWAY, J. R. & BURNHAM, C. W., 1972. Melting relations of basalt with equilibrium water pressure less than total pressure. *Journal of Petrology* **13**, 1-29.

HOUSEMAN, G. A., MCKENZIE, D. P. & MOLNAR, P. 1981. Convective instability of a thickened boundary layer and its relevance for the thermal evolution of continental convergent belts. *Journal of Geophysical Research* **86**, 6115-6132.

HUANG, H. Q., LI, X. H., LI, W. X. & LI, Z. X. 2011. Formation of high $\delta^{18}O$ fayalite-bearing A-type granite by high temperature melting of granulitic metasedimentary rocks, southern China. *Geology* **39**, 903-906.

HUVELIN, P. 1977. Etude géologique et gîtologique du massif hercynien des Jebilet (Maroc occidental). *Notes et Mémoires Service Géologique Maroc* **232 bis**, 1-307.

JIANG, Y. H., ZHAO, P., ZHOU, Q., LIAO, S. Y. & GIN, G. D. 2009. Middle to late Jurassic felsic and mafic magmatism in southern Hunan province, southeast China. Implications for continental arc to rifting. *Lithos* **107**, 185-204.

KEPPLER, H., 1996. Constraints from partitioning experiments on the compositions of subduction-zone fluids. *Nature* **380**, 237–240.

KERR, A. & FRYER, B. J. 1993. Nd isotope evidence for crust-mantle interaction in the generation of A-type granitoid suites in Labrador, Canada. *Chemical Geology* **104**, 439-60.

LAGARDE, J. L. 1989. Granites tardi carbonifères et déformation crustale : l'exemple de la meseta marocaine. *Mémoires et documents du Centre Armoricain d'Etude Structurale des Socles* **26**, 1-342.

LAGARDE, J. L. & CHOUKROUNE, P. 1982. Cisaillement ductile et granitoïdes syntectoniques : l'exemple du massif hercynien des Jebilet (Maroc). *Bulletin de la Société Géologique de France* **7**, 299-307.

LAGARDE, J. L. & MICHARD, A. 1986. Stretching normal to the regional thrust displacement in a thrust-wrench shear zone, Rehamna massif, Morocco. *Journal of Structural Geology* **8**, 483-492.

LAGARDE, J. L., AÏT OMAR, S. & RODDAZ, B. 1990. Structural characteristics of syntectonic plutons with special reference to late carboniferous plutons from Morocco. *Journal of Structural Geology* **12**, 805-821.

LAGARDE, J. L., CAPDEVILA, R. & FOURCADE, S. 1992. Granites et collision continentale : l'exemple des granitoïdes carbonifères dans la chaîne hercynienne ouest-européenne. *Bulletin de la Société Géologique de France* **163**, 597-610.

LAMB, S., HOKE, L., KENNAN, L. & DEWEY, J. 1997. Cenozoic evolution of the central Andes in Bolivia and northern Chile. In *Orogeny through Time* (eds J.P. Burg & M. Ford), pp. 237-264, Geological Society of London, Special Publication no 121.

LANDENBERGER, B. & COLLINS, W. J. 1996. Derivation of A-type granites from a dehydrated charnokitic lower crust: evidence from the Chaelundi complex, Eastern Australia. *Journal of Petrology* **37**, 145-170.

LEAT, P. T., JACKSON, S. E., THORPE, R. S. & STILLMAN, C. J. 1986. Geochemistry of bimodal basalt-subalkaline/peralkaline rhyolite provinces within the Southern British Caledonides. *Journal of the Geological Society of London* **143**, 259-273.

LE CORRE, C. & BOULOTON, J. 1987. Un modèle de 'structure en fleur' associant décrochement et convergence : Les Jebilet centro-occidentales (Maroc hercynien). *Comptes Rendus de l'Académie des Sciences, Paris* **13**, 751-755.

LE CORRE, C. & SAQUAQUE, A. 1987. Comportement d'un système pluton-encaissant dans un champ de déformation régional : le granite de Bramram (Jebilet, Maroc hercynien). *Bulletin de la Société Géologique de France* **4**, 665-673.

LINDSLEY, D. H. & ANDERSEN, D. J., 1983. A two pyroxene thermometer. Proceeding of the thirteenth lunar and planetary science confernce, Part 2. *Journal of Geophysical Research* **8**, supplement A887-A906.

LITVINOVSKY, B. A., JAHN, B. M., ZANVILEVICH, A. N., SAUNDERS, A., POULAIN, S., KUZMIN, D. V., REICHOW, M. K. & TITOV, A. V. 2002. Petrogenesis of syenite–granite suites from the Bryansky Complex (Transbaikalia, Russia): implications for the origin of A-type granitoid magmas. *Chemical Geology* **189**, 105-133.

LOOSVELD, R. J. H. & ETHERIDGE, M. A. 1990. A model for low-pressure metamorphism during crustal thickening. *Journal of Metamorphic Geology* **8**, 257-267.

MAHÉO, G., GUILLOT, J., BLICHERT-TOFT, Y., ROLLAND, Y. & PECHER, A. 2002. A slab break-off model for the Neogene thermal evolution of South Karakorum and South Tibet. *Earth and Planetary Science Letters* **195**, 45-58.

MAHMOOD, A. & BENNANI, A. 1984. S-type characteristics of the Hercynian granitoids of the Central Paleaozoic massif, Morocco. *Geological Magazine* **121**, 301-309.

MAYOL, S. & MULLER, J. 1985. Mise en évidence d'une unité allochtone hercynienne précoce (antéschisteuse) dans les Jebilet occidentales (Maroc). Etude de structuration de la zone de contact. *Comptes Rendus de l'Académie des Sciences, Paris* **300**, 369-372.

McBirney, A. 1989. The Skaergaard Layered Series: I. Structure and Average Compositions. *Journal of Petrology* **30**, 363-397.

Michard, A., 1976. Eléments de géologie marocaine. *Notes et Mémoires Service Géologique Maroc* **252**, 1-458.

Michard, A., Soulaimani, A. Hoepffner, C. Ouanaimi, H. Baidder., L. Rjimati, E.C. & Saddiqi, O. 2010. The South-Western Branch of the Variscan Belt : Evidence from Morocco. *Tectonophysics* **492**, 1-24.

Mitjavila, J., Marti, J., Soriano, C., 1997. Magmatic evolution and tectonic setting of the Iberian Pyrite Belt volcanism. *Journal of Petrology* **38**, 727-755.

Miyashiro, A., 1974. Volcanic rock series in island arcs and active continental margins. *American Journal of Science* **274**, 321-355.

Mrini, Z., Rafi, A., Duthou, J. L. & Vidal, P. 1992. Chronologie Rb-Sr des granitoïdes hercyniens du Maroc : conséquences. *Bulletin de la Société Géologique de France* **163**, 281-291.

Mushkin, A., Navon, O., Halicz, L., Hartmann, G. & Stein, M. 2003. The petrogenesis of A-type magmas from the Amram Massif, southern Israel. *Journal of Petrology* **44**, 815-832.

Nelson, K. D. 1992. Are crustal thickness variations in old mountain belts like the Appalachians a consequence of lithospheric delamination? *Geology* **20**, 498-502.

N'Diaye, I., Essaifi, A., Dubois, M., Goodenough, K. & Boyce, A. Geology, fluid inclusion and sulphur isotope evidence for syntection mineralisation in the Kettara deposit. Implications for genesis of the massive sulphide deposits of the Jebilet massif (Morocco). *Submitted to Mineralium Deposita*.

PATIÑO DOUCE, A. E. 1997. Generation of metaluminous A-type granites by low-pressure melting of calc-alkaline granitoids. *Geology* **25**, 743-746.

PEARCE, J. A. 1983. The role of sub-continental lithosphere in magma genesis at destructive plate margins. In *Continental basalts and mantle xenoliths* (Eds. C. J. Hawkesworth & M. J. Norry), pp. 230-249. Nantwich: Shiva.

PEARCE, J. A., HARRIS, N. B. W. & TINDLE, A. G. 1984. Trace element discrimination diagrams for the tectonic interpretation of granitic rocks. *Journal of Petrology* **25**, 956-923.

PIQUÉ, A., JEANNETTE, D. & MICHARD, A. 1980. The western meseta shear zone, a major and permanent feature of the Hercynian belt in Morocco. *Journal of Structural Geology* **2**, 397-410.

PIQUÉ, A. & MICHARD, A. 1989. Moroccan hercynides : a synopsis. The palaeozoic sedimentary and tectonic evolution at the northern margin of west Africa. *American Journal of Science* **289**, 286-330.

PIQUÉ, A., BOSSIÈRE, G., BOUILLIN, J. P., CHALLOUAN, A. & HOEPFFNER, C. 1993. Southern margin of the variscan belt: the north-western Gondwana mobile zone (Eastern Morocco and Northern Algeria). *Geologische Rundschau* **82**, 432-439.

PLAYFORD, G., GONZALEZ, F., MORENO, C. & ALANSARI, A. 2008. Palynostratigraphy of the Sarhlef Series (Mississippian), Jebilet Massif, Morocco. *Micropaleontology* **54**, 89-124

RODDAZ, M., BRUSSET, S., SOULA, J. C., BEZIAT, D., BENABBOU, M., DEBAT, P., DRIOUCH, Y., CHRISTOPHOUL, F., NTARMOUCHANT, A. & DERAMOND, J., 2002. Foreland basin magmatism in the western Moroccan Meseta and geodynamic inferences. *Tectonics* **21**, 1043-1065.

ROLLINSON, H. 1993. *Using geochemical data: evaluation, presentation, interpretation*. Longman Scientific & Technical, Harlow, 352 pp.

SAMSON, S. D., HIBBARD, J. P. & WORTMAN, G. L. 1995. Nd isotopic evidence for juvenile crust in the Carolina terrane, southern Appalachians. *Contributions to Mineralogy and Petrology* **121**, 171–184.

SEYFERTH, M. & HENK, A. 2004. Syn-convergent exhumation and lateral extrusion in continental collision zones: insights from three-dimensional numerical models. *Tectonophysics* **382**, 1-29.

SKJERLIE, K. P. & JOHNSTON, A. D. 1993. Fluid absent melting behavior of an F-rich tonalitic gneiss at mid-crustal pressures: Implications for the generation of anorogenic granites. *Journal of Petrology* **34**, 785-815.

SPULBER, S. D. & RUTHERFORD, M. J. 1983. The origin of rhyolite and plagiogranite in oceanic crust: An experimental study. *Journal of Petrology* **24**, 1-25.

SMITH, D.R., NOBLETT, J., WOBUS, R.A., UNRUH, D., DOUGLASS, J., BEANE, R., DAVIS, C. GOLDMAN, S., KAY, G., GUSTAVSON, B., SALTOUN, B. & STEWART, J. 1999. Petrology and geochemistry of late-stage intrusions of the A-type, mid-Proterozoic Pikes Peak batholith (Central Colorado, USA): implications for petrogenetic models. *Precambrian Research* **98**, 271–305.

SUN, S. & MCDONOUGH, W. F. 1989. Chemical and isotopic systematic of oceanic basalts: implications for mantle composition and processes. In *Magmatism in the Ocean Basins* (eds A. D. Saunders & M. J. Norry), pp. 313-345, Geological Society of London, Special Publication no 42.

TAYLOR, S.R. AND MCLENNAN, S.M. 1995. The geochemical evolution of the continental crust. *Reviews of Geophysics* **33**, 241–265.

THOMPSON, R.N., DICKIN, A.P., GIBSON, I.L. & MORRISON, M.A. 1982. Elemental fingerprints of isotopic contamination of Hebridean Palaeocene mantle-derived magmas by Archaean sial. *Contributions to Mineralogy and Petrology* **79**, 159–168.

THORPE, R. S. LEAT, P. T., MANN, A. C., HOWELLS, M. F., REEDMAN, A. J. & CAMPBELL, D. G. 1993. Magmatic evolution of the ordovician Snowdon volcanic centre, North Wales (UK). *Journal of Petrology* **34**, 711-714.

TOTTEN, M. W., HANAN, M. A. WEAVER B. L. 2000. Beyond whole-rock geochemistry of shales: The importance of assessing mineralogic controls for revealing tectonic discriminants of multiple sediment sources for the Ouachita Mountain flysch deposits. *Geological Society of America Bulletin* **112**, 1012–1022.

TURNER, S., FODEN, J. D. & MORRISSON, R. S. 1992. Derivation of some A-type magmas by fractionation of basaltic magmas: an example from the Pathdaway ridge. South Australia. *Lithos* **28**, 151-179.

TURNER, S., PLATT, J. P., GEORGE, R. M. M., KELLY, S. P., PEARSON, D. G. & NOWELL, G. M. 1999. Magmatism associated with orogenic collapse of the Betic-Alboran Domain, SE Spain. *Journal of Petrology* **40**, 1011-1036.

VOGEL, T. A., WILLIAMS, E. R., PRESTON, J. K. & WALKER, B. M. 1976. Origin of the late Palaeozoic plutonic massifs in Morocco. *Geological Society of America Bulletin* **87**, 1753-1762.

VON RAUMER, J.F. & STAMPFLI, G.M. 2008. The birth of the Rheic Ocean: early Palaeozoic subsidence patterns and subsequent tectonic plate scenarios. *Tectonophysics* **46**, 9–20.

VON RAUMER, J.F., BUSSY, F. & STAMPFLI, G.M. 2009. The Variscan evolution in the External Massifs of the Alps and place in their Variscan framework. *Comptes Rendus Geosciences*. **341**, 239–252.

WANG, K. L., CHUNG, S. L., O'REILLY, S. Y., SUN, S. S., SHINJO, R. & CHEN, C. H. 2004. Geochemical constraints for the genesis of postcollisional magmatism and the geodynamic evolution of the northern Taiwan region. *Journal of Petrology* **45**, 975-1011.

WATSON, E. B. & HARRISON, T. M. 1983. Zircon saturation revisited: temperature and composition effects in a variety of crustal magma types. *Earth and Planetary Science Letters* **64**, 295-304.

WHALEN, J. B., CURRIE, K. L. & CHAPPELL, B. W. 1987. A-type granites: geochemical characteristics, discrimination and petrogenesis. *Contributions to Mineralogy and Petrology* **95**, 407-419.

WHALEN, J. B., MCNICOLL, V. J., VAN STAAL, C. R., LISSENBERG, C. J., LONGSTAFFE, F. J., GENNER, G. A. & VAN BREEMAN, O. 2006. Spatial, temporal and geochemical characteristics of Silurian collision-zone magmatism, Newfoundland Appalachians: an example of a rapidly evolving magmatic system related to slab break-off. *Lithos* **89**, 377-404.

WICKHAM, S. M., ALBERTS, A. D., ZANVILEVICH, A. N., LITVINOVSKY, B. A., BINDEMAN, I. N. & SCHAUBLE, E. A. 1996. A Stable isotope study of anorogenic magmatism in East Central Asia. *Journal of Petrology* **37**, 1063-1095.

WILSON, M., 1989. *Igneous petrogenesis*. Unwin Hyman, London, 456 pp.

WINCHESTER, J. A. & FLOYD, P. A., 1976. Geochemical magma type discrimination: application to altered and metamorphosed basic igneous rocks. *Earth and Planetary Science Letters* **28**, 459-469.

WOOD, D. A. 1980. The application of a Th–Hf–Ta diagram to problems of tectonomagmatic classification and to establishing the nature of crustal contamination of basaltic lavas of the BritishTertiary volcanic province. *Earth and Planetary Science Letters* **50**, 11–30.

YANG, J. H., WU, F. Y., CHUNG, S. L., WILDE, S. A. & CHU, M. F. 2006. A hybrid origin for the Qianshan A-type granite, Northeast China: geochemical and Sr–Nd–Hf isotopic evidence. *Lithos* **89**, 89-106.

Figure Captions

Figure 1. (a) Moroccan Variscan granitoids (black) and their Palaeozoic cover (gray) (TN: Tanncherfi, AB : Aouli-Bou Mia, TZ : Tazekka, TC : Tichka, MC : Maroc Central with Zaer (Z), Oulmes (O) and Ment (M) plutons, R : Rehamna, G: Guemassa). (**b**) Geological sketch map of the Jebilet massif (modified from Huvelin, 1977). Slip on the regional fractures is accompanied by extrusion to the South of the central Jebilet block (large white arrow). BHD refer to Koudiat Bouzlaf, Hamra and Diab intrusions, respectively, DH (Draa El Harach), KK (Koudiat Kettara), OH (Oled Har), SF (Safsafat), SH (Sarhlef), EH (El Harcha), EM (El Mna), JB (Jbel Bouzlaf), CJP (Central Jebilet Pluton), EJP (Eastern Jebilet Pluton).

Figure 2. Low Pressure-High Temperature metamorphism around (**a**) the BHD granophyric microgranites (modified from Essaifi *et al.*, 2001) and (**b**) the Eastern Jebilet cordierite-bearing granodioritic pluton (modified from A. Chemesseddoha, unpub. Ph.D. thesis, Univ. Rennes I, Rennes, 1986). **Location of the Sr-Nd samples is indicated. The other samples were collected from Kettara intrusion (GSK, DK13, DK23, DK30, GK3, MK5 and DK25 mafic-ultramafic rocks; MTK and MGTK microgranites), Oled Har intrusion (OH6 and 00M03 gabbros; MOH1 and 00M04 microgranites), El Mna (EM4 gabbro, EM7 quartz-diorite and EM6 microgranite), Jbel Bouzlaf intrusion (BZN3 and MBZN3 microgranites) and Central Jebilet Pluton (00M01 granodiorite) (see Fig. 1b).**

Figure 3. (Colour online) Field photos of the Jebilet magmatism. (a) view within the Kettara mafic-ultramafic layered intrusion showing Upper Visean metaturbidites (hV) cropping out in anticline window overlaid by ultramafic cumulates (UM) and leucogabbors (LCG); (b-e) outcrops of the Kettara intrusion showing (b) cm-scale layering in the ultramafic cumulates; scale piece is 58 mm across, (c) a rapidly chilled and weakly folded doleritic dyke

crosscutting ultramafic cumulates, (d) a felsic dyke crosscutting ultramafic cumulates and enclosing mafic enclaves, (e) the mafic enclaves are elongated and occur most abundantly at the intrusive contact, decreasing rapidly towards the centre of the dyke; (f) mafic enclaves within quartz-diorite in the Jbel Bouzlaf intrusion; scale piece is 22 mm across, g) view showing an E-W cross section of the Koudiat Bouzlaf microgranites (μγ) enclosing synplutonic mafic dykes (δ) and intruding Upper Visean metaturbidites; (h-i) outcrops of the cordierite-bearing granodiorite of the Eastern Jebilet Pluton showing (h) a dark magmatic microgranular enclave and (i) a large xenocryst of andalusite. Scale piece is 22 mm across.

Figure 4. Harker plots for selected major and trace elements of the Jebilet plutonic rocks. CaO, Al_2O_3, MgO and Fe_2O_3* contents of the main fractionating minerals in the mafic-ultramafic cumulates are also plotted, Ol (Olivine), PLG (Plagioclase), CPX (Clinopyroxene).

Figure 5. (a, b) Plot of Mg# and K_2O vs. SiO_2 for the Carboniferous Jebilet intrusive rocks. A silica gap exists between the mafic-ultramafic rocks and the granitoids where the scatter of data points is related postmagmatic mobilisation of K, Mg and/or Fe. The original data for the granodiorites and leucogranites are from El Amrani El Hassani (1996). (c) Plot of the Jebilet mafic-ultramafic rocks in the FeO*/MgO vs. SiO_2 diagram of Miyahiro (1974). Data points show a Fe-enriched trend.

Figure 6. (a) Plot of TiO_2 vs. Zr/P_2O_5 for non-cumulate mafic rocks of the Jebilet bimodal intrusive rocks. (b) Total Fe_2O_3 vs. TiO_2 diagram for the non-cumulate mafic rocks compared with fields for experimental peridotite melts (Falloon *et al.*, 1988).

Figure 7. (a) SiO_2 vs. ASI [molar $Al_2O_3/(CaO+Na_2O+K_2O)$] index, **(b)** (Na+K+2Ca)/(Al*Si) (cation ratio) vs. Zr diagram (after Watson and Harrison, 1983). Symbols as in Fig. 4.

The original data for the granodiorites are from El Amrani El Hassani (1996).

Figure 8. Chondrite-normalised REE plot for representative rocks of the Jebilet magmatism (a) mafic- ultramafic rocks, (b) granophyric microgranites, (c) cordierite-bearing granodiorites. Normalising values are from Evensen *et al.* (1978). Primitive mantle-normalised trace element diagrams for representative rocks of the Jebilet magmatism (d) mafic- ultramafic rocks, (e) granophyric microgranites, εNd_{330} values of the microgranites in the corresponding intrusions are indicated, (f) cordierite-bearing granodiorites. Normalising values are from Sun and McDonough (1989). The original data for the granodiorites and leucogranites are from El Amrani El Hassani (1996).

Figure 9. Initial $^{87}Sr/^{86}Sr$ vs. initial εNd values of the Jebilet plutonic rocks. The granitoids of the Tichka plutonic complex are also plotted. A mixing curve between the mafic end member deduced for the Tichka plutonic complex (Gasquet *et al.*, 1992) [$(^{87}Sr/^{86}Sr)i$ = 0.7027, Sr = 700 ppm, Nd=20 ppm, εNd_i = +7.6] and a bulk-sediment corresponding to the mean composition of the protolith from which most of the granites in Morocco were derived [$(^{87}Sr/^{86}Sr)i$ = 0.718, εNd_i = -9, Sr = 150 ppm, Nd = 30 ppm] is shown. The bar represents $(^{87}Sr/^{86}Sr)_{330}$ of the country rocks. Also shown are the fields of MORB and OIB (Wilson, 1989).

The original data for the Jebilet granodiorites and leucogranites are from Z. Mrini, unpub. Ph.D. thesis, Univ. Clermont Ferrand, Clermont Ferrand, 1985, and those for the Tichka plutonic complex from Gasquet *et al.* (1992).

Figure 10. Mg# (as a differentiation index) vs. $\varepsilon Nd_{(330)}$ in the Jebilet mafic-ultramafic rocks. The observed evolutionary trend (arrow) is consistent with mixing or Assimilation and Fractional Crystallisation (AFC) process between a mafic end member represented by GSK sample (Mg# = 7 and $\varepsilon Nd_{(330)}$ = + 8.7) and an upper crustal end member (bulk-sediment with Mg# = 4 and $\varepsilon Nd_{(330)}$ = -9).

Figure 11. **(a) Plots of the Jebilet intrusives in the classification diagram of Frost *et al.* (2001)**, (b) Plots of the Jebilet microgranites (circles) and quartz-diorites (triangles) in the Zr vs. 10000 Ga/Al diagram of Whalen *et al.* (1987) showing affiliation with A-type granites; (c) Nb–Y–Ga ternary diagram for the subdivision into A_1- and A_2-type granites (Eby, 1992). Symbols are as in figure 4.

Figure 12. Trace-element concentrations of the Sarhlef schists normalised to upper custal values (Taylor & McLennan, 1985), and compared to expected patterns of sediments in active-margin settings and passive-margin settings, after Floyd (1991). (unpublished data, A. Essaifi)

Figure 13. (a) Plot of initial εNd values vs. Nd concentrations.

Figure 14. (a) Distribution of the Jebilet mafic rocks in the Th-Hf-Ta discrimination diagram of Wood (1980). (b) Plot of Th/Yb vs. Ta/Yb. Vectors shown indicate the influence of subduction components (S), within-plate enrichment (W), crustal contamination (C) and fractional crystallisation (F). Dashed lines separate the boundaries of the tholeiitic (TH), calc-alkaline (CA) and shoshonitic (SH) fields (after

Pearce, 1983). Original data from F. Kharbouch, unpub. Ph.D. thesis, Univ. Bretagne occidentale, Brest, 1994. The mafic rocks of Table 1 are also included in (a) considering the ratios Nb/Ta=16 and Zr/Hf=39.

Figure 15. Cartoons showing crust-mantle interaction and subsequent melting and intrusion of Carboniferous granitic and gabbroic intrusions of the Moroccan Mesetas. (a) Westward subduction, partial melting of the lithospheric mantle and generation of potassic to shoshonitic granitic intrusions in the eastern Meseta at about 350 Ma. (b) Cessation of subduction at about 330 Ma, syn-convergence extension and exhumation of intermediate P/T metamorphic rocks, upwelling of asthenospheric melts, convective removal of the lithospheric mantle, partial melting in the shallow crust and generation of coeval A-type granitic magmas and cordierite-bearing granodioritic plutons. (c) Progressive replacement of the lithosphere by the asthenosphere leading to generation of leucogranites of purely crustal origin at about 300 Ma.

Table 1. Major (wt %) and trace element (ppm) data of representative samples from the intrusive rocks of the Jebilet massif.

	Ultramafic and mafic cumulates						Non-cumulate mafic rocks					
Rock type	Prd	Prd	Lcb	Lcb	Lcb	Lcb	Trt	μGab	Dol	μGab	Dol	Dol
Sample	DK13	DK14	DK30	GK2	GK3	EM4	GSK	OH6	BBN	DK23	BKD	BBS
Location	KK	KK	KK	KK	KK	EM	KK	OH	JB	KK	BHD	BHD
SiO_2	40.07	40.78	44.98	48.07	44.72	51.14	46.98	49.99	48.79	48.09	49.77	50.38
Al_2O_3	7.28	7.66	21.39	19.53	19.91	18.65	14.48	15.32	15.41	15.4	14.53	14.43
Fe_2O_3*	9.88	9.5	7.59	4.3	5.48	7.16	9.39	10.43	10.44	10.34	11.3	11.41
MnO	0.17	0.15	0.11	0.08	0.1	0.14	0.16	0.16	0.18	0.18	0.22	0.2
MgO	28.27	28.35	8.33	8.12	10.95	5.92	11.83	7.88	7.76	9.89	7.39	7.04
CaO	5.22	4.25	11.21	15.25	11.24	10.41	11.42	11.07	10.68	10.22	10.67	10.82
Na_2O	0	0	1.34	1.63	1.2	2.69	1.25	2.11	2.02	1.83	1.82	2.58
K_2O	0.06	0.04	0.82	0.26	1.17	0.89	0.27	0.69	1.09	0.21	1.02	0.37
TiO_2	0.4	0.49	0.55	0.36	0.5	0.94	0.78	1.54	1.4	1.34	1.31	1.35
P_2O_5	0.03	0.04	0.04	0.04	0.05	0.09	0.07	0.16	0.13	0.14	0.13	0.11
L.O.I.	8.49	8.44	3.47	1.84	4.1	1.43	2.2	0.9	2.06	2.26	1.48	0.75
total	99.87	99.7	99.83	99.48	99.42	99.46	98.83	100.24	99.96	99.9	99.64	99.44
Nb	4	1	1	4	5	7	4	7	5	4	7	7
Zr	27	31	37	36	47	84	49	103	90	100	89	88
Y	6	7	12	6	11	24	20	36	32	29	34	31
Sr	15	11	187	212	341	241	67	144	177	158	131	131
Rb	6	6	65	21	77	37	19	38	31	12	56	10
Co	97	97	46	25	41	23	46	41	46	45	39	43
V	89	101	113	107	93	204	212	288	273	259	312	313
Ni	1132	1386	223	145	358	54	327	107	72	217	40	33
Cr	2002	2015	264	1041.5	1018.5	414	721	333	303	460	140	115
Ba	13	19	36	37	33	101	11	108	222	76	118	322
Ga	7	7	14	12	12	18	15	18	17	17	17	18
Cu	3	23	66	102	51	17	†	29	58	57	11	53
Zn	61	62	43	31	43	53	†	56	80	77	66	128
Th	<1	<1	1	<1	<1	2	†	2	<1	2	<1	<1
Pb	<1	<1	1	1	2	2	†	3	5	<1	3	9
La	0.66	0.76	†	0.77	1.32	†	1.11	†	4.44	6.52	6.17	7.02
Ce	2.14	1.77	†	2.35	3.87	†	3.59	†	12.72	16.11	16.71	17.79
Pr	0.38	0.44	†	0.41	0.65	†	0.67	†	2.03	2.28	2.35	2.53
Nd	2.09	2.3	†	2.31	3.39	†	3.92	†	10.31	11.29	10.96	11.74
Sm	0.81	0.8	†	0.86	1.16	†	1.53	†	3.36	3.5	3.35	3.51
Eu	0.35	0.34	†	0.42	0.52	†	0.69	†	1.21	1.14	1.1	1.23
Gd	1.05	1.38	†	1.18	1.5	†	2.39	†	4.32	4.34	4.19	4.4
Tb	0.18	0.2	†	0.21	0.26	†	0.41	†	0.75	0.68	0.74	0.77
Dy	1.2	1.28	†	1.44	1.83	†	2.88	†	4.5	4.43	5.03	5.24
Ho	0.27	0.31	†	0.3	0.38	†	0.68	†	1.05	1,00	1.06	1.11
Er	0.71	0.85	†	0.82	1.08	†	1.72	†	2.93	2.81	3.02	3.19
Yb	0.75	0.81	†	0.77	1.02	†	1.83	†	2.75	2.59	2.88	3.05
Lu	0.11	0.15	†	0.12	0.15	†	0.31	†	0.42	0.4	0.45	0.47
ASI	0.76	0.99	0.91	0.64	0.84	0.77	0.63	0.63	0.64	0.71	0.62	0.59
Mg#	0.85	0.86	0.68	0.79	0.8	0.62	0.71	0.6	0.6	0.65	0.56	0.55

Table 1 (continued)

	Quartz-diorites			Microgranites								
Rock type	Q-D	Q-D	Q-D	μGr	μGr	TTg	TTg	TTg	μGr	TTg	μGr	TTg
Sample	OH4	EM7	MBZN5	KAZ	TBZ	M23	B34	B35	B45	DD1	EM6	MBZN4
Location	OH	EM	JB	BHD	BHD	BHD	BHD	BHD	BHD	BHD	EM	JB
SiO2	63.69	59.52	60.62	74.48	74.4	75.43	76.19	77.4	74.17	77.01	70.14	77.58
Al_2O_3	15.39	13.11	14.55	12.39	12.33	12.52	12.29	13.15	12.32	12.65	13.09	12.9
Fe_2O_3*	5.09	12.11	7.22	2.92	4.18	2.87	2.01	0.59	2.77	1.25	2.45	1.41
MnO	0.07	0.17	0.11	0.04	0.03	0.04	0.03	0.02	0.04	0.02	0.05	0.03
MgO	2	1.18	2.74	0.2	0.15	0.3	0.19	0.06	0.12	0.21	0.17	0.07
CaO	6.86	5.67	7.34	1.78	1.13	2.43	2.1	2.73	1.03	3.01	4.55	0.37
Na_2O	4.22	3.71	4.06	2.78	3.94	3.42	3.46	3.94	2.46	3.78	4.81	6.8
K_2O	0.34	0.92	0.56	3.85	2.27	1.13	1.48	0.72	4.98	0.47	0.63	0.42
TiO_2	1.1	1.52	1.13	0.22	0.25	0.23	0.21	0.25	0.25	0.22	0.51	0.17
P_2O_5	0.24	0.47	0.11	0.04	0.04	0.04	0.04	0.04	0.04	0.05	0.06	0.02
L.O.I.	0.58	0.87	1.5	0.53	0.7	0.96	0.98	0.53	0.87	0.72	2.72	0.49
total	99.59	99.25	99.94	99.23	99.42	99.37	98.98	99.43	99.05	99.39	99.18	100.26
Nb	19	23	10	22	23	20	19	21	22	20	23	17
Zr	539	454	216	316	335	315	272	317	343	269	839	241
Y	70	99	42	105	106	94	89	92	95	81	115	69
Sr	283	145	325	170	126	262	256	332	126	290	214	153
Rb	16	37	8	103	86	51	46	20	143	22	34	9
Co	16	21	19	5	9	10	6	1	7	3	6	2
V	139	<1	211	0	0	8	7	6	7	5	<1	7
Ni	16	8	16	3	4	2	2	1	2	1	12	3
Cr	54	10	39	11	7	15	8	6	14	19	20	11
Ba	139	289	228	930	524	177	468	103	1083	135	191	155
Ga	22	23	22	21	21	21	19	15	20	18	23	21
Cu	5	12	10	4	<1	3.5	2.26	1.9	2	2.1	5	<1
Zn	27	86	55	34	33	29	22	10	24	13	23	13
Th	18	18	8	31	30	32	32	33	31	32	27	18
Pb	5	13	4	6	2	5	7	4	5	1	†	2
La	†	†	†	†	†	71.05	67.59	67.08	66.51	56.86	†	49.44
Ce	†	†	†	†	†	151.89	157.76	149.24	146.28	131.79	†	111.75
Pr	†	†	†	†	†	18.56	17.84	17.91	17.38	16.17	†	13.64
Nd	†	†	†	†	†	71.59	70.54	72.56	67.3	61.63	†	52.88
Sm	†	†	†	†	†	15.72	15.55	16.93	15.22	13.89	†	12.45
Eu	†	†	†	†	†	1.31	1.33	1.43	1.52	1.61	†	1.03
Gd	†	†	†	†	†	14.6	14.87	16.41	14.37	13.19	†	12.03
Tb	†	†	†	†	†	2.47	2.46	2.7	2.41	2.22	†	2.06
Dy	†	†	†	†	†	14.98	15.34	16.74	14.51	14.06	†	13.09
Ho	†	†	†	†	†	3.03	3.18	3.46	3.08	3,00	†	2.64
Er	†	†	†	†	†	8.56	8.89	8.1	8.51	8.25	†	7.65
Yb	†	†	†	†	†	9.3	9.25	8.86	8.61	10.49	†	8.1
Lu	†	†	†	†	†	1.42	1.43	1.39	1.31	1.52	†	1.23
ASI	0.78	0.75	0.71	1.03	1.12	1.11	1.11	1.08	1.09	1.04	0.78	1.05
Mg#	0.44	0.16	0.43	0.12	0.07	0.17	0.16	0.17	0.08	0.25	0.12	0.09

Table 1 (continued)

					Granodiorites††					Leucogranites††		
Rock type	µGr	µGr	TTg	µGr	Grd	Grd	Grd	Grd	Grd	Lgr	Lgr	Lgr
Sample	OH1	MOH1	MTK	MBZN3	J.1.1	J.4.7	J.4.20	J.2.4	J.2.24	J.4.14	J.4.21	J.OZ.9
Location	OH	OH	KK	JB	CJP	CJP	CJP	EJP	EJP	CJP	EJP	EJP
SiO2	75.57	73.77	76.19	76.09	70.26	71.07	69.44	67.89	66.86	74.7	75.99	76.34
Al_2O_3	13.63	13.55	12.98	12.52	13.91	14.04	14.47	15.37	16	13.37	13.12	13.01
Fe_2O_3*	0.82	2.77	1.5	1.6	4.71	3.6	3.79	4.18	3.71	0.72	0.86	0.56
MnO	0.01	0.03	0.02	0.02	0.05	0.06	0.06	0.05	0.07	0.21	0.01	0.02
MgO	0.36	0.39	0.51	0.11	0.81	0.8	1.06	1.33	1.3	0.21	0.18	0.07
CaO	2.76	3.02	2.99	0.88	1.36	1.58	0.92	1.75	1.73	0.43	0.34	0.37
Na_2O	5.37	4.28	3.99	3.91	2.5	2.53	2.27	2.6	3.58	2.46	2.18	3.55
K_2O	0.29	0.82	0.23	3.12	4.72	4.3	5.03	4.28	3.88	6.04	5.82	4.24
TiO_2	0.38	0.42	0.3	0.15	0.49	0.46	0.55	0.6	0.53	0.12	0.08	0.04
P_2O_5	0.21	0.25	0.07	0.01	0.13	0.15	0.15	0.19	0.18			
L.O.I.	0.43	0.47	0.43	1.24	0.95	0.57	1.29	1.01	1.25	0.81	0.49	0.77
total	99.83	99.77	99.21	99.65	99.89	99.16	99.03	99.25	99.09	99.07	99.07	98.97
Nb	18	19	18	19	†	†	†	†	†	†	†	†
Zr	315	313	380	235	134	60	70	48	42	†	†	†
Y	74	72	95	93	34	23	33	21	21	†	†	†
Sr	264	322	379	232	89	81	98	190	450	55	43	127
Rb	11	76	15	56	†	†	†	†	†	†	†	†
Co	4	10	6	0.5	52	56	59	63	53	46	†	43
V	19	22	11	9	54	53	63	73	59	†	†	†
Ni	5	6	8	3	13	11	12	16	28	†	†	†
Cr	39	25	16	6	31	30	38	53	46	†	†	†
Ba	105	258	127	1271	60	370	844	670	815	152	105	168
Ga	18	20	17	21	†	†	†	†	†	†	†	†
Cu	<1	2.9	†	4.3	†	†	†	†	†	†	†	†
Zn	8	24	†	30	†	†	†	†	†	†	†	†
Th	19	23	†	21	†	†	†	†	†	†	†	†
Pb	5	7	†	8	†	†	†	†	†	†	†	†
La	65.91	51.43	†	65.75	39.1	34.3	35.8	39.4	28	†	†	†
Ce	139.73	120.58	†	132.39	86.8	71	77.2	83.6	59.7	†	†	†
Pr	15.91	13.85	†	16.69	9.4	7.97	8.56	9.05	6.23	†	†	†
Nd	60.01	54.9	†	66.08	36.6	31.1	33.4	34.6	25.6	†	†	†
Sm	13.15	12.03	†	14.93	8.33	7.26	7.36	7.33	5.6	†	†	†
Eu	1.15	1.17	†	1.49	0.78	0.76	1.09	1.06	1.05	†	†	†
Gd	12.95	12.01	†	14.75	7.88	7.05	6.74	6.43	4.87	†	†	†
Tb	2.09	1.94	†	2.33	†	†	†	†	†	†	†	†
Dy	12.98	11.58	†	14.61	8.05	7.93	6.18	6.19	4.47	†	†	†
Ho	2.59	2.3	†	3.11	†	†	†	†	†	†	†	†
Er	7.15	6.6	†	9.09	4.65	4.59	3.37	3.49	2.53	†	†	†
Yb	6.22	6.45	†	9.1	4.45	4.47	3.2	3.35	2.42	†	†	†
Lu	0.85	0.94	†	1.33	0.67	0.66	0.48	0.52	0.37	†	†	†
ASI	0.96	1.01	1.06	1.1	1.19	1.2	1.33	1.27	1.21	1.18	1.25	1.17
Mg#	0.47	0.22	0.4	0.12	0.25	0.31	0.36	0.39	0.41	0.37	0.29	0.2

ASI = molar Al_2O_3/(CaO+Na_2O+K_2O); Mg# = molar Mg/(Mg+Fe); For locations see Fig, 1b; *Total Fe calculated as Fe_2O_3; †not available; ††The original data for granodiorites and leucogranites are from El Amrani El Hassani (1996). Abbreviations : Prd: peridotite; Trt: troctolite; Lcb: leucogabbro; Q-D: Quartz-diorite; µGab: microgabbro; Dol : dolerite; µGr: granophyric microgranite; TTg: trondhjemite/tonalite gneiss; Grd: granodiorite; Lgr: leucogranite.

Table 2. Rb, Sr, Sm and Nd concentrations (ppm), Sr and Nd isotopic ratios of the intrusive rocks of the Jebilet massif

Sample	Location	Rock type	Rb	Sr	$^{87}Rb/^{86}Sr$	$^{87}Sr/^{86}Sr$	± 2σ	$(^{87}Sr/^{86}Sr)_i$	Sm	Nd	$^{147}Sm/^{144}Nd$	$^{143}Nd/^{144}Nd$	± 2σ	ε Nd $_{(T)}$	TDM (Ma)
GK2	KK	CPX	0.37	15.88	0.067	0.704787	6	0.70448	1.33	2.65	0.3044	0.513237	8	7.2	*
GSK	KK	Trt	20.8	65.7	0.916	0.707867	7	0.70367	1.86	4.68	0.24	0.513178	4	8.7	*
DK13	KK	Prd	6.56	12.98	1.463	0.711337	8	0.70463			†	†			
DK23	KK	µGab	12.4	149	0.241	0.707341	8	0.70624	3.56	11.9	0.1809	0.512771	4	3.3	*
DK30	KK	Lcb	65	187	1.006	0.711388	8	0.70666	1.08	3.25	0.2003	0.513003	9	7,0	*
GK3	KK	Lcb	77.3	332.5	0.673	0.711756	8	0.70867			†	†			
MK5	KK	Lcb	83.5	94.8	2.55	0.717165	10	0.70547			†	†			
DK25	KK	Prd	1.525	6.44	0.685	0.709952	9	0.70681			†	†			
00M03	OH	Gab			†	†		†	4.97	17.1	0.1753	0.512828	7	4.6	*
OH6	OH	µGab	38	144	0.764	0.707836	8	0.70425	4.08	13.5	0.1833	0.512844	5	4.6	*
EM4	EM	Lcb	37	241	0.444	0.708887	8	0.7068	2.87	10.1	0.171	0.512712	4	2.5	*
EM7	EM	Q-D	37	145	0.738	0.710727	9	0.70726	14.7	60	0.1482	0.512505	4	-0.6	1500
B45	BHD	µGr	153	127	3.492	0.72556	10	0.70954	14.71	65.4	0.1361	0.512376	4	-2.6	1519
01M24	BHD	µGr			†	†		†	14.3	64.3	0.1344	0.512343	7	-3.1	1550
KAZ	BHD	µGr	103†	170†	1.75	0.71863	8	0.7106			†	†			
TBZ	BHD	µGr	86	126	1.97	0.72053	8	0.71149			†	†			
B34	BHD	TTg	49.2	268	0.532	0.713682	7	0.71124	14.7	65.47	0.1358	0.512358	4	-2.9	1548
3DI	BHD	µGr	88.69	124.72	2.06	0.719472	5	0.71002			†	†			
B44	BHD	µGr	94.7	189.6	1.446	0.71799	5	0.71136			†	†			
M24	BHD	µGr	71.99	198.68	1.049	0.715354	9	0.71054			†	†			
DD1	BHD	TTg	22	292.9	0.217	0.711702	6	0.71071			†	†			
MOH1	OH	µGr	83.8	322	0.754	0.715	7	0.71154	12.43	54.77	0.1372	0.512188	4	-6.3	1913
00M04	OH	µGr			†	†			11.4	50.4	0.1372	0.512194	5	-6.2	1901
EM6	EM	µGr	34	214	0.46	0.710066	8	0.70791	17	70.2	0.1462	0.512496	4	-0.6	1476
MBZN3	JB	µGr	61.5	238	0.748	0.714747	8	0.71132	14.89	65.29	0.1379	0.512474	4	-0.7	1359
BZN3	JB	TTg	127	67	5.499	0.734452	8	0.70863		53.2		0.512505	5		
MTK	KK	TTg	15	379	0.114	0.71238	7	0.71186			†	†			
MGTK	KK	TTg	3	348	0.025	0.711856	9	0.71174			†	†			
00M01	CJP	Grd			†	†			7.27	32.3	0.1359	0.512250	4	-4.8	1761
01M23	EJP	Grd			†	†			7.2	35.8	0.1215	0.512200	5	-5.4	1569

Table 2 (continued)

Sample	Location	Rock type	Rb	Sr	$^{87}Rb/^{86}Sr$	$^{87}Sr/^{86}Sr$	± 2σ	$(^{87}Sr/^{86}Sr)_i$	Sm	Nd	$^{147}Sm/^{144}Nd$	$^{143}Nd/^{144}Nd$	± 2σ	ε Nd $_{(T)}$	TDM (Ma)
JO3	EJP††	Grd	168	307	1.58	0.71419	†	0.7068	6.17	31.2	0.12038	0.51219	†	-5.5	1566
JO9	EJP††	Grd	171	175	2.85	0.72336	†	0.710	6.85	35.8	0.11647	0.51217	†	-5.8	1535
JO12	EJP††	Grd	142	338	1.28	0.7123	†	0.7063	6.41	32.99	0.11827	0.51228	†	-3.7	1389
JO13	EJP††	Grd	178	230	2.25	0.71863	†	0.7081	7.53	38.48	0.11933	0.5122	†	-5.3	1533
JO15	EJP††	Grd	117	679	0.499	0.70637	†	0.704	2.44	13.09	0.11346	0.51249	†	0.6	1005
JO16	EJP††	Grd	110	642	0.496	0.70652	†	0.7042	2.42	12.84	0.1147	0.51251	†	1	987
JO21	EJP††	Mme	67.9	318	0.618	0.7078	†	0.7049	8.43	40.69	0.12611	0.51242	†	-1.3	1271
JO25	EJP††	Mme	30.6	541	0.164	0.70494	†	0.7042	3.19	14.23	0.13646	0.51272	†	4.1	850
JTa1	CJP††	Grd	268	78.4	9.94	0.75458	†	0.7079	8.12	38.71	0.12759	0.51222	†	-5.2	1644
JTa4	CJP††	Grd	163	219	2.15	0.72058	†	0.7105	8.29	40.15	0.12568	0.51227	†	-4.2	1523
JBa4	CJP††	Mme	245	89	7.98	0.74821	†	0.7108	9.79	48.14	0.12379	0.51223	†	-4.9	1558
JBa5	CJP††	Grd	301	57.5	15.3	0.77866	†	0.707	8.37	41.85	0.12174	0.51221	†	-5.2	1557
JBr1	CJP††	Grd	264	118	6.48	0.73876	†	0.7076	8.61	41.87	0.12517	0.51214	†	-6.7	1736
JO17	CJP††	Lgr	242	54.3	13	0.77261	†	0.7117	6.03	33.42	0.11019	0.5121	†	-7.2	1545
JBr5	CJP††	Lgr	259	36.4	20.7	0.80455	†	0.7177	1.31	4.52	0.17642	0.51235	†	-4.9	3253

Depleted mantle model age (TDM) calculated following the model of DePaolo (1981a). *Samples with $^{147}Sm/^{144}Nd$ > 0.16 do not provide meaningful models; †not available; ††Original data from Z. Mrini, unpub. Ph.D. thesis, Univ. Clermont Ferrand, Clermont Ferrand, 1985. Abbreviations: Cpx: clinopyroxene separate from a gabbro; Mme: Mafic magmatic enclave; the other abbreviations are as in Table 1.

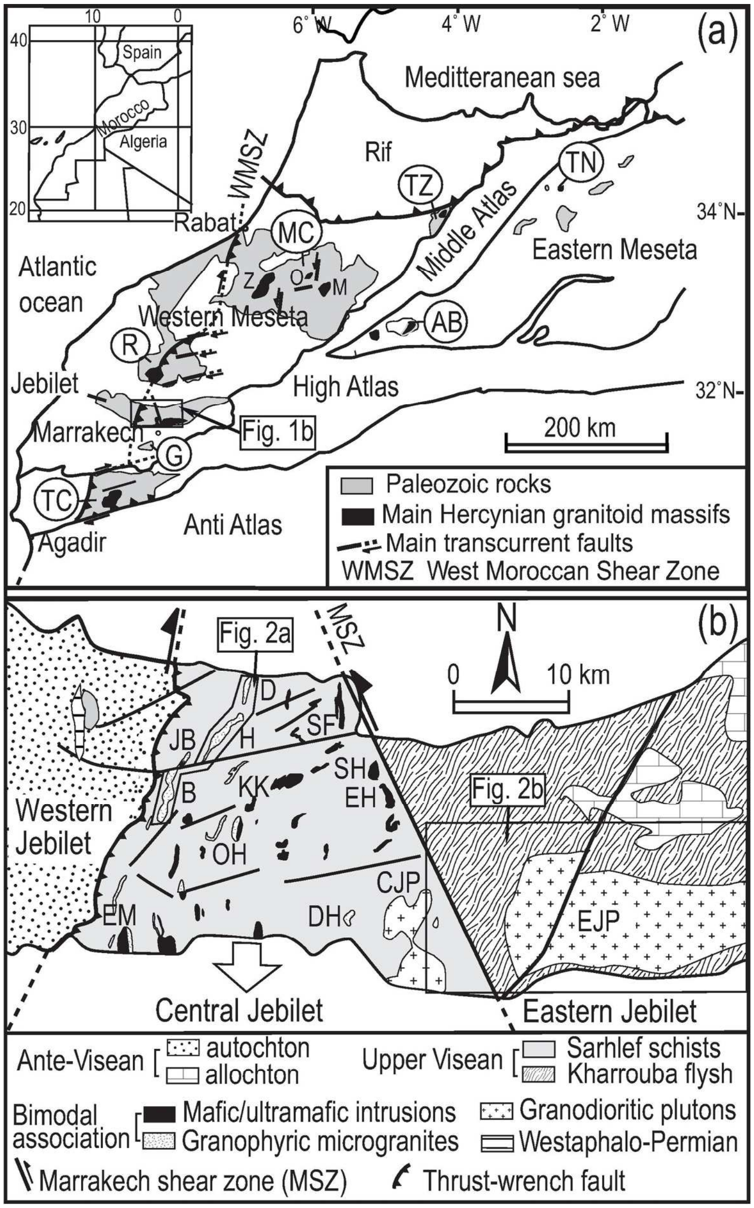

Fig. 1
128x206mm (300 x 300 DPI)

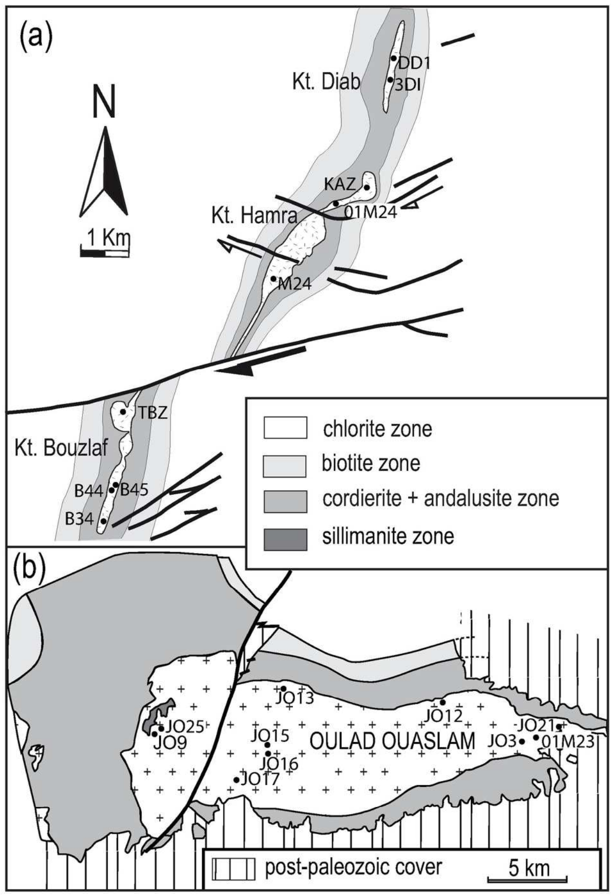

Fig. 2
157x210mm (300 x 300 DPI)

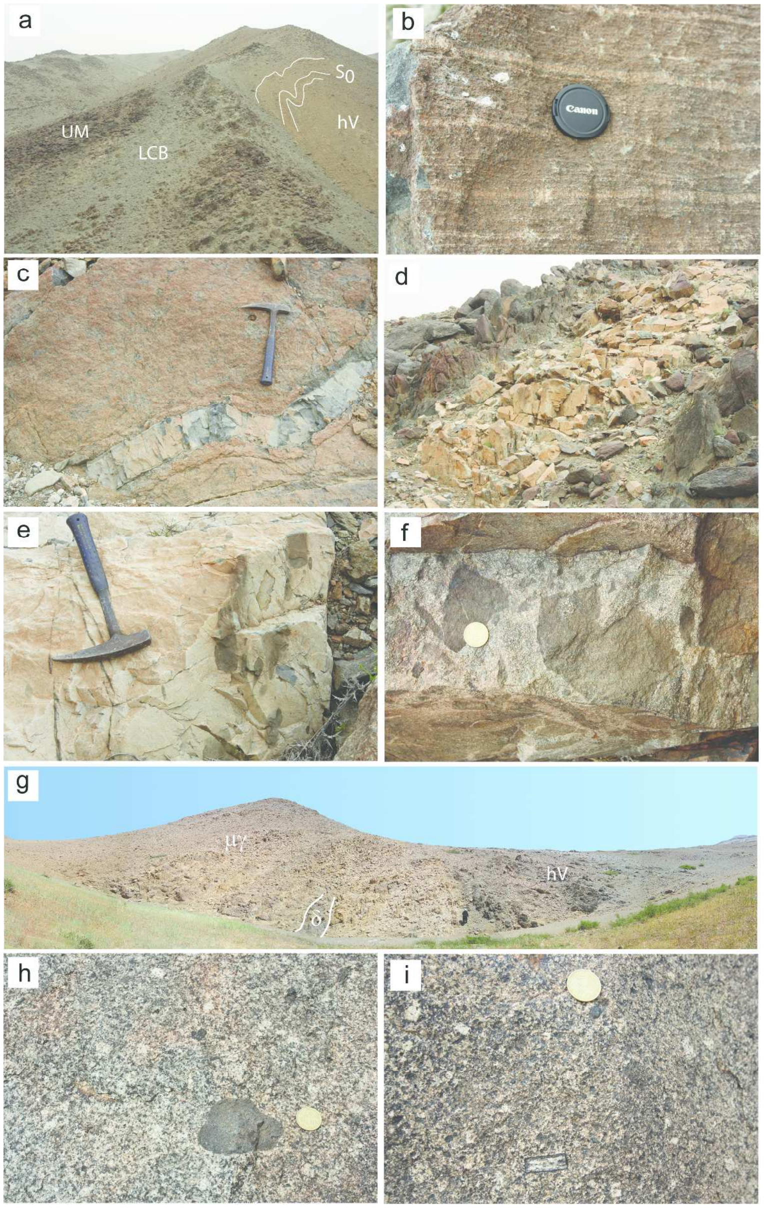

Fig. 3
235x372mm (300 x 300 DPI)

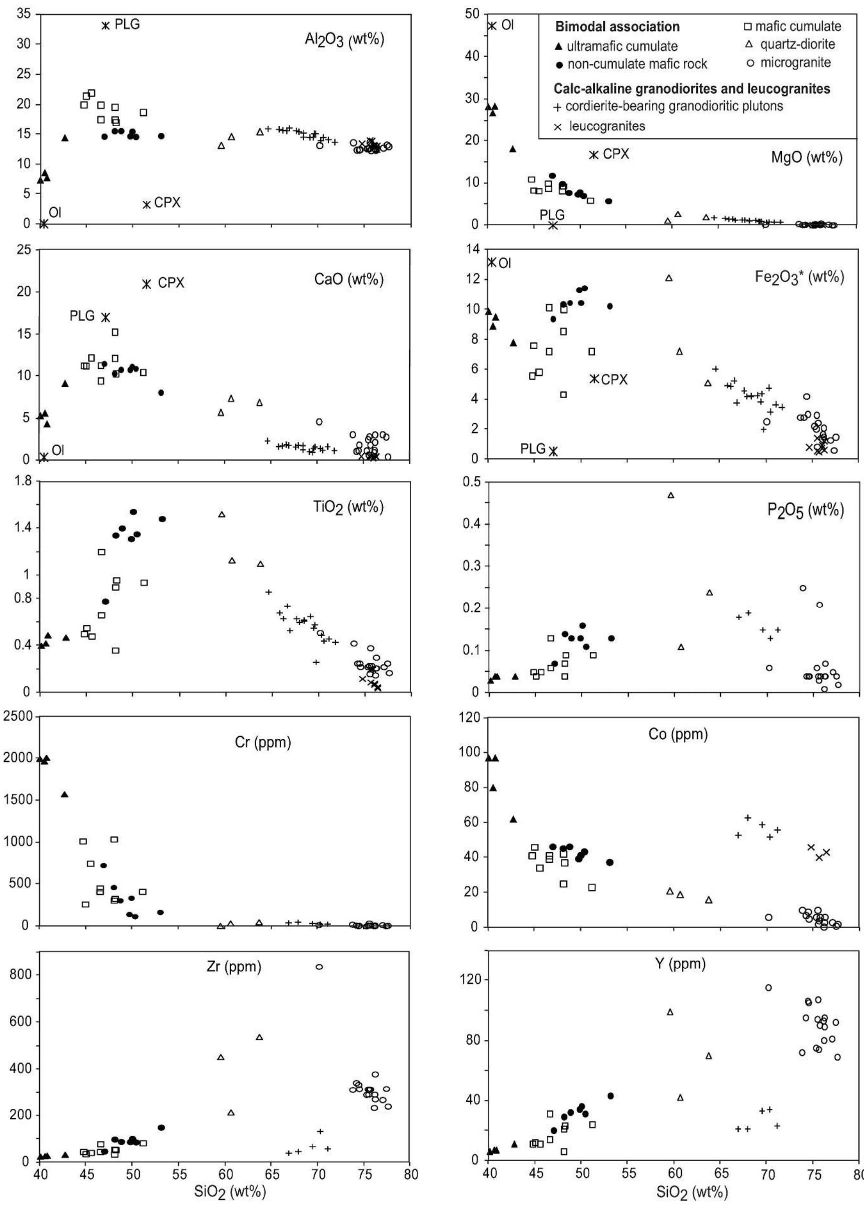

Fig. 4
237x329mm (300 x 300 DPI)

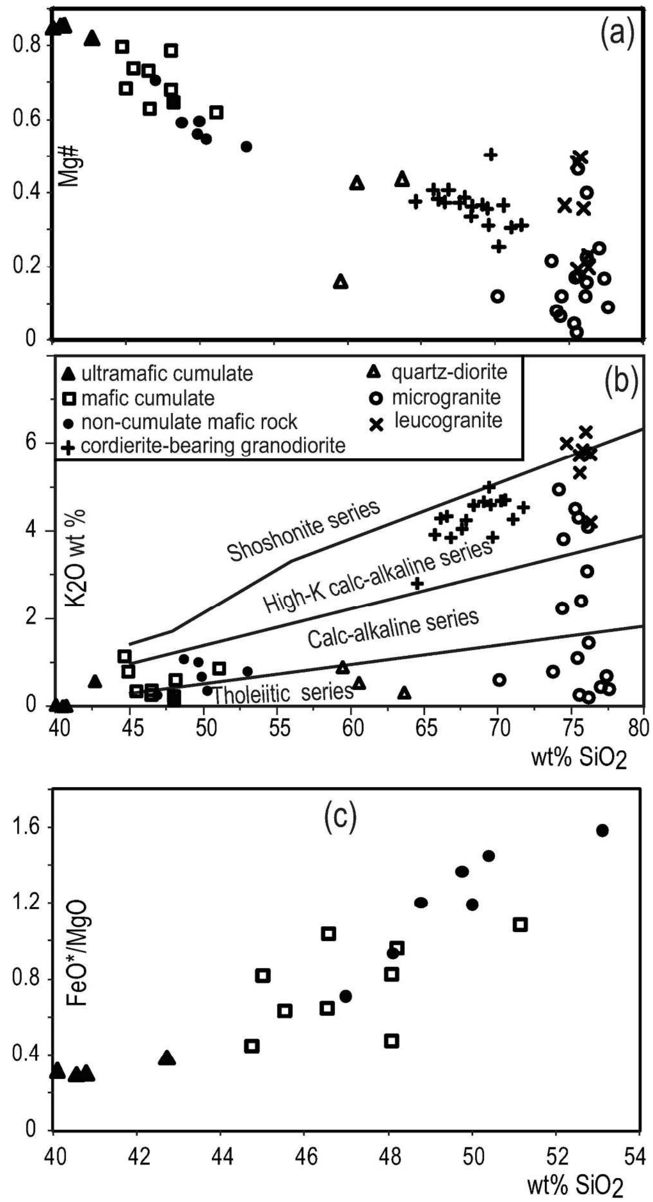

Fig. 5
153x287mm (300 x 300 DPI)

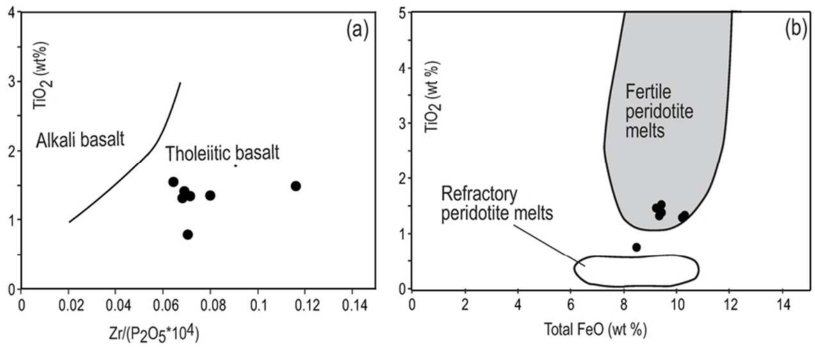

Fig. 6
91x42mm (300 x 300 DPI)

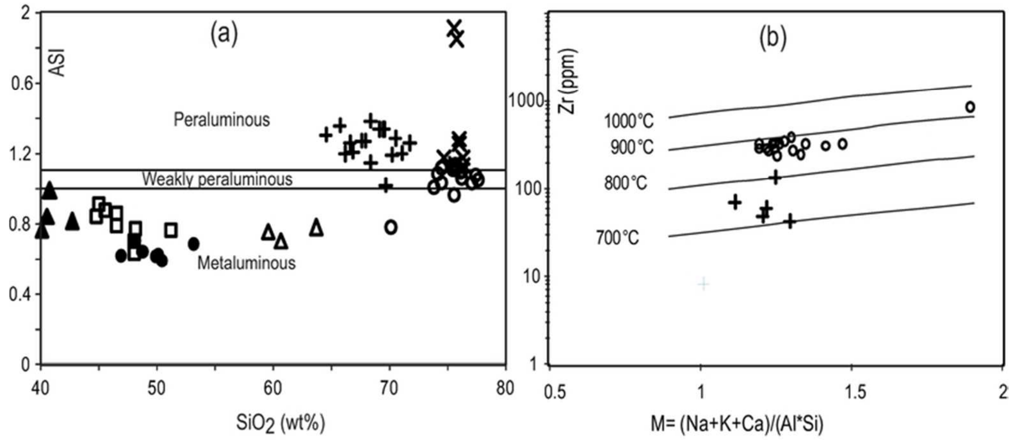

Fig. 7
70x30mm (300 x 300 DPI)

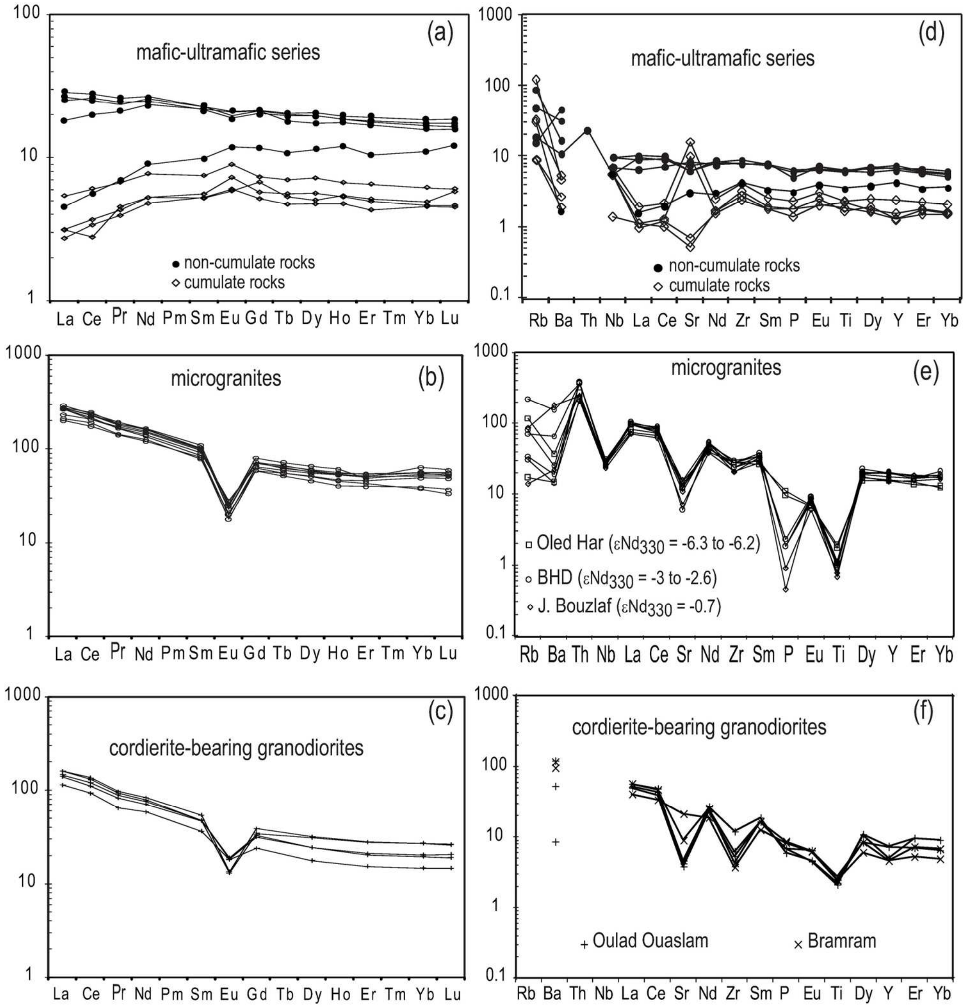

Fig. 8
169x170mm (300 x 300 DPI)

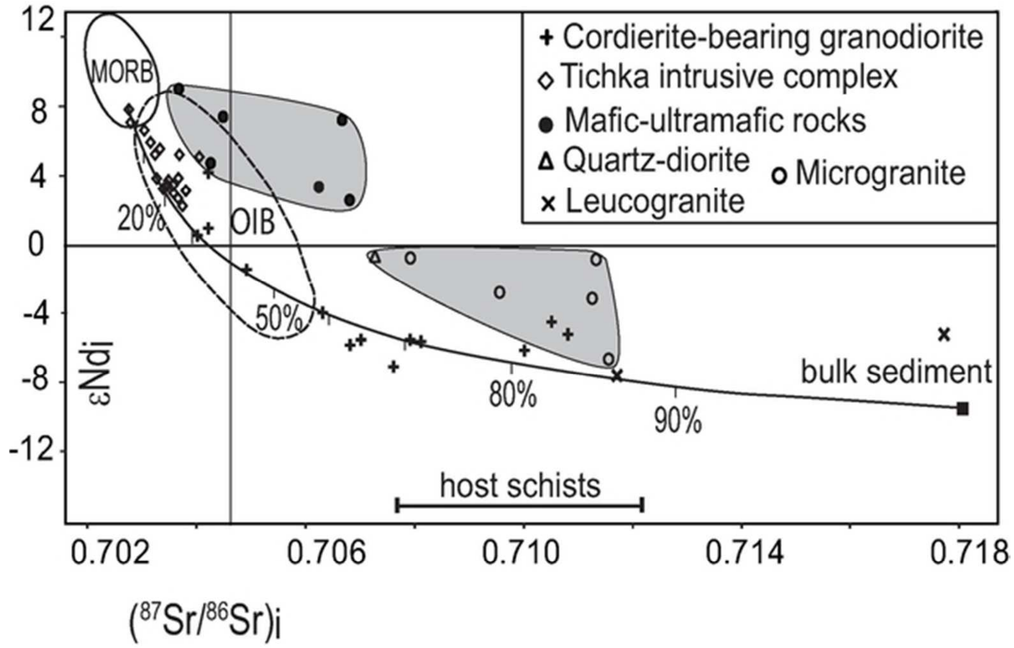

Fig. 9
53x34mm (300 x 300 DPI)

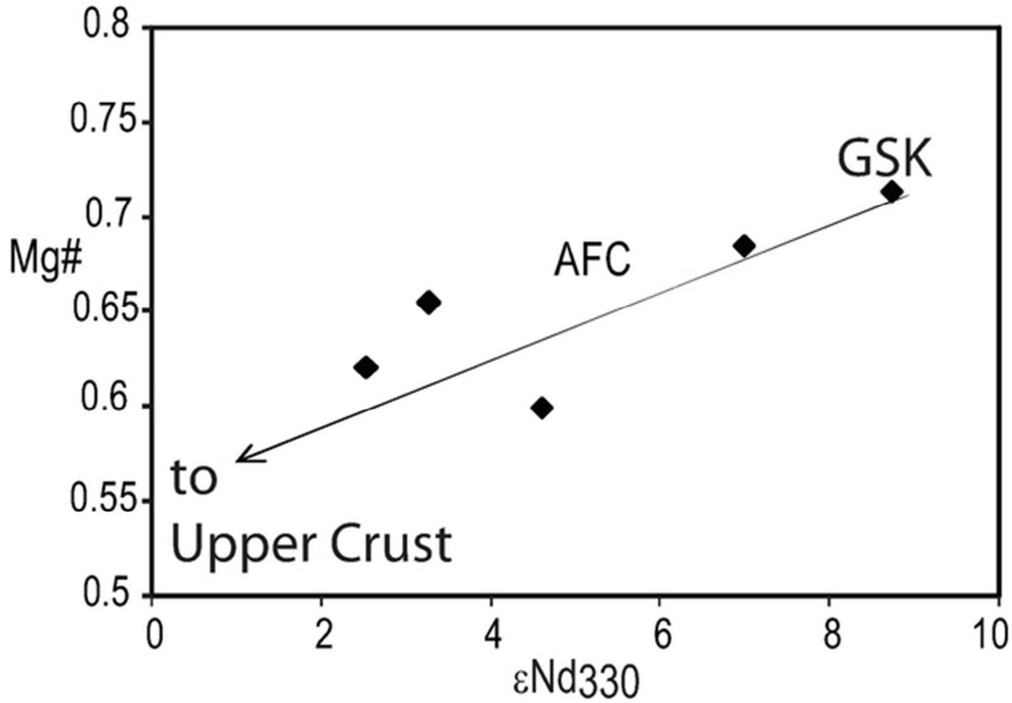

Fig. 10
53x38mm (300 x 300 DPI)

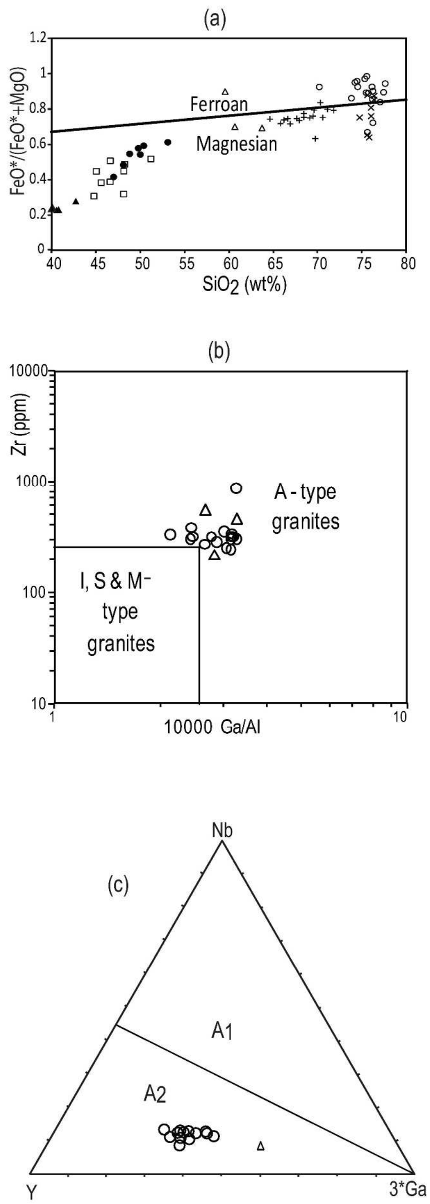

Fig. 11
202x576mm (300 x 300 DPI)

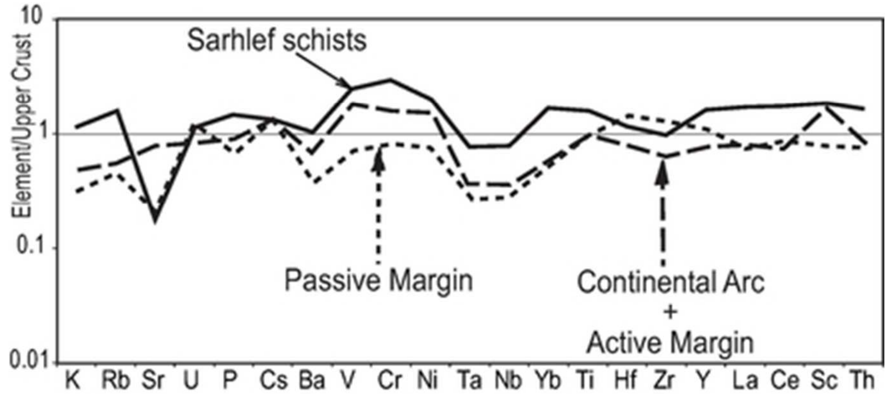

Fig. 12
37x17mm (300 x 300 DPI)

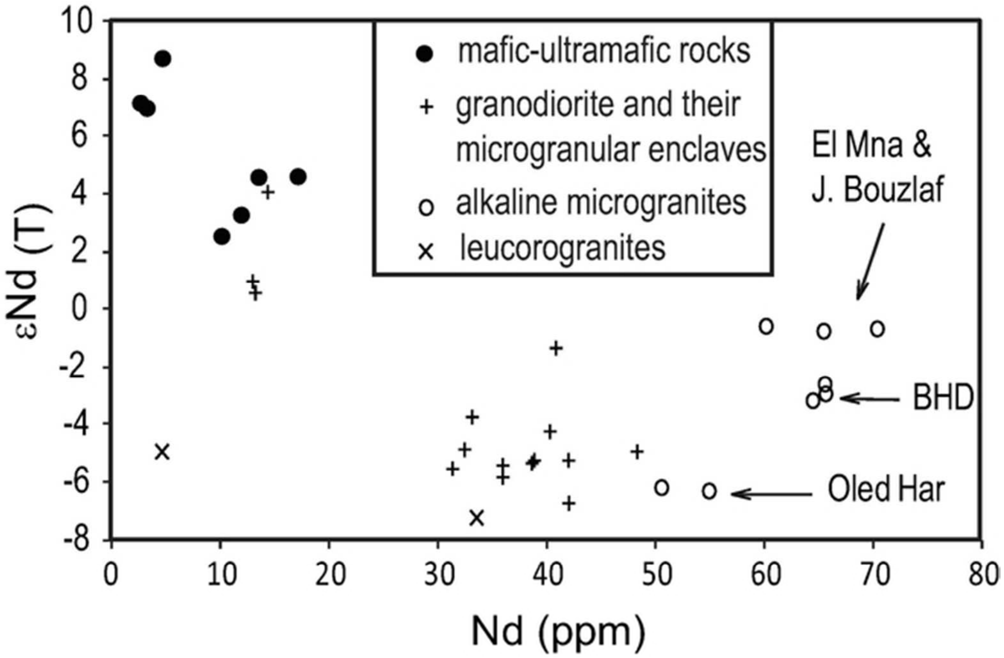

Fig. 13
55x36mm (300 x 300 DPI)

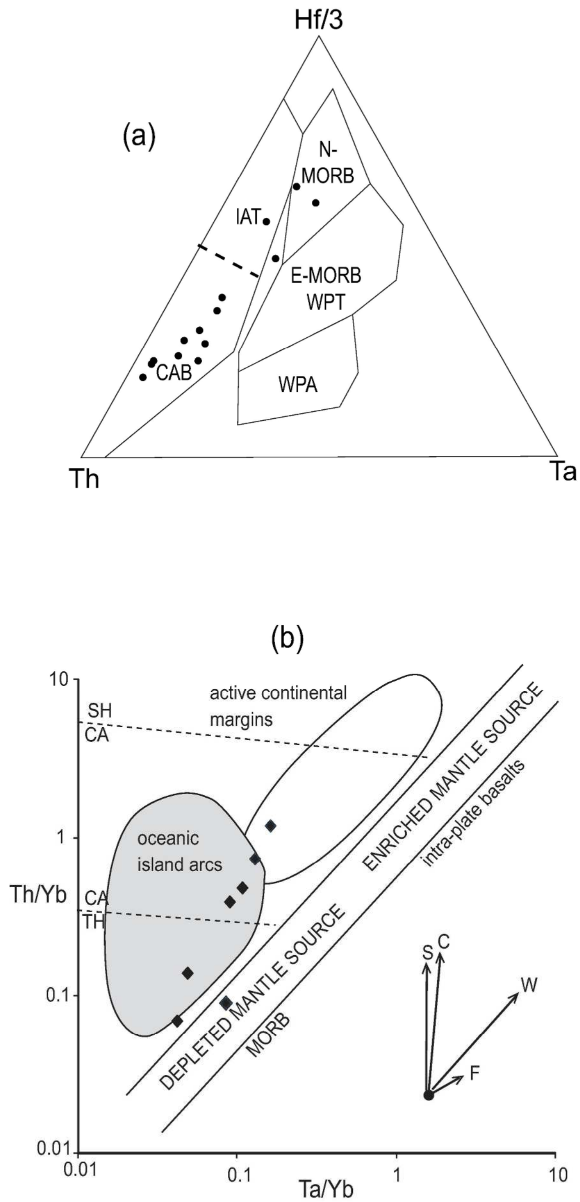

Fig. 14
170x359mm (300 x 300 DPI)

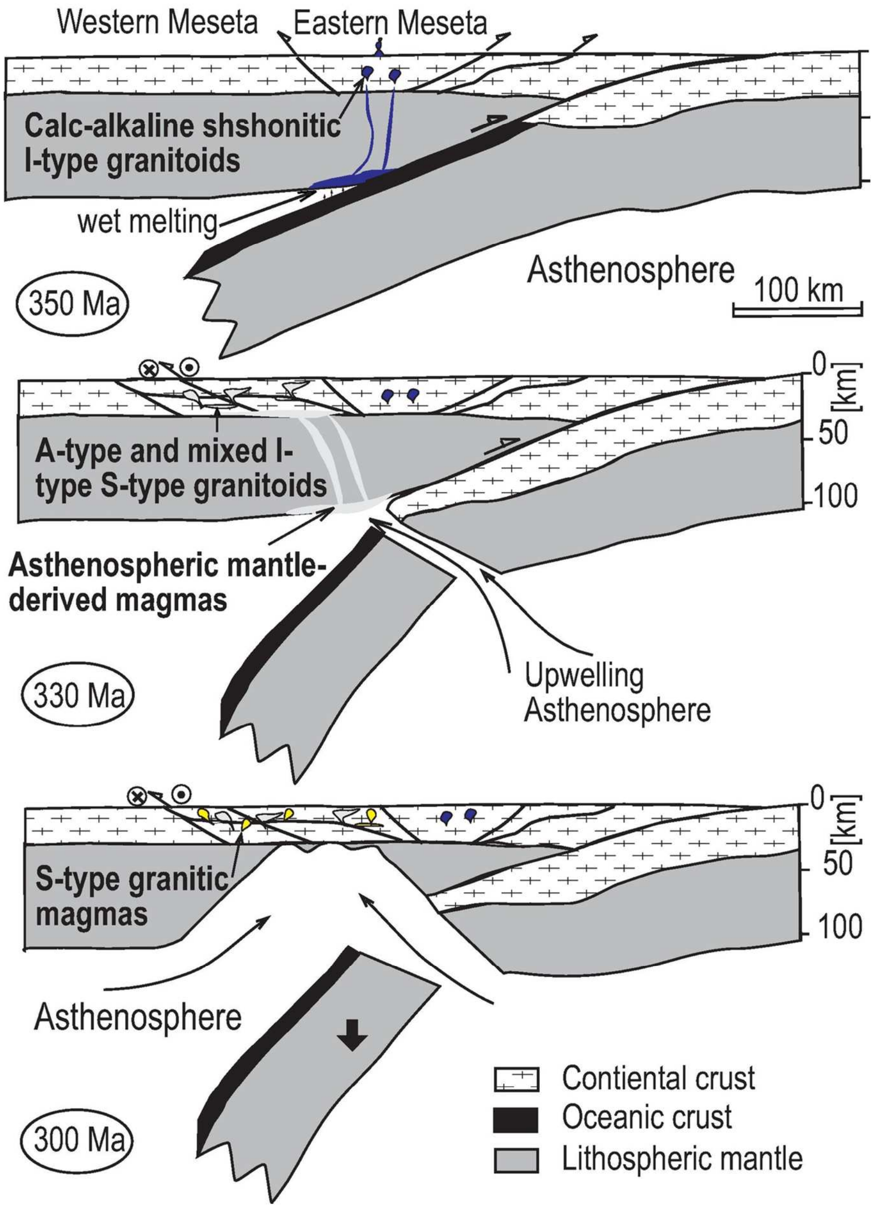

Fig. 15
109x151mm (300 x 300 DPI)